JOURNAL OF GEOPHYSICAL RESEARCH, VOL. 104, NO. D24, PAGES 30,853–30,883, DECEMBER 27, 1999

Comparisons of aircraft, ship, and buoy meteorological measurements from TOGA COARE

Sean P. Burns,[1] Djamal Khelif,[1] Carl A. Friehe,[1,2] Alastair G. Williams,[3] Phil Hignett,[4] Alan L. M. Grant,[3] Jörg M. Hacker,[5] David P. Rogers,[6] E. Frank Bradley,[7] Robert A. Weller,[8] Meghan F. Cronin,[9] Steven P. Anderson,[8] Chris W. Fairall,[10] and Clayton A. Paulson[11]

Abstract. Comparisons of mean ambient temperature, specific humidity, static pressure, and horizontal wind from the five Tropical Ocean-Global Atmosphere Coupled Ocean-Atmosphere Response Experiment (TOGA COARE) boundary layer aircraft were obtained from 38 two- and three-aircraft, close-formation, level runs. These, together with consideration of surface measurements from buoys and ships, led to proposed empirical corrections for the aircrafts temperature, humidity, and pressure measurements, minimizing the systematic errors between the aircraft data sets. The aircraft-measured winds were also compared. The TOGA COARE bulk flux algorithm was used to extrapolate the low-level aircraft data to the individual ship and buoy sensor heights for 267 overflight comparisons. In addition, all low-level aircraft data and corresponding ship and buoy data from boundary layer missions were extracted and adjusted to a 10-m reference height. The recommended aircraft corrections bring the aircraft-ship-buoy data sets into better agreement, resulting in a consistent data set for air-sea interaction analyses. Frequency distributions of the 10-m aircraft, ship, and buoy data from the boundary layer missions also agree.

1. Introduction

The Coupled Ocean-Atmosphere Response Experiment (COARE) was designed as part of the Tropical Ocean-Global Atmosphere (TOGA) program to study the energy exchange and coupling between the atmosphere and the ocean in the western Pacific warm pool region [*Webster and Lukas,* 1992]. Five research aircraft were used during the intensive observing period (IOP) of COARE between November 1, 1992 and February 28, 1993, to measure the mean and turbulent structure of the boundary layer. The aircraft data provide a vital connection between data from ships, buoys, soundings, and satellites. In order to successfully integrate the data from these disparate sources, comparisons are required and corrections must be determined so that a consistent aircraft data set can be produced for future analysis. The goals of this paper are to (1) determine corrections for the aircraft data based on aircraft wingtip-to-wingtip comparisons and consideration of the ship and buoy data, (2) adjust the low-level aircraft overflight data down to the levels of the ship and buoy data for comparison, and (3) compare the extrapolated 10-m aircraft, ship, and buoy data for the entire IOP. The corrections for the aircraft data are based on consideration of many comparisons and factors; sometimes subjective decisions had to be made due to unexplained changes in particular sensors and conditions. For a few variables, a date-dependent correction had to be used. The low-level aircraft boundary layer data are necessarily limited to daylight hours in generally fair weather conditions.

A good preliminary summary of COARE scientific findings is in the work of *Godfrey et al.* [1998], although it should be noted that they list undocumented differ-

[1]Department of Mechanical and Aerospace Engineering, University of California, Irvine.
[2]Also at Department of Earth System Science, University of California, Irvine.
[3]Hadley Centre for Climate Prediction and Research, Berkshire, United Kingdom.
[4]Meteorological Support Group/DG(R&T), Ministry of Defence, London, United Kingdom.
[5]Flinders Institute for Atmospheric and Marine Sciences, Adelaide, Australia.
[6]Scripps Institution of Oceanography, La Jolla, California.
[7]Commonwealth Scientific and Industrial Research Organization Land and Water, Canberra, Australia.
[8]Woods Hole Oceanographic Institution, Woods Hole, Massachusetts.
[9]Pacific Marine Environmental Laboratory, Seattle, Washington.
[10]Environmental Technology Laboratory, Boulder, Colorado.
[11]College of Oceanic and Atmospheric Sciences, Oregon State University, Corvallis.

Paper number 1999JD900934.
0148-0227/99/1999JD900934$09.00

Table 1. Instrumentation of Aircraft and Surface Platforms Used in the TOGA COARE Mean Quantity Data Comparisons

Platform	Wind System	Air Temp[a]	Humidity[b]	SI[c]
		Research Aircraft		
NOAA WP-3D N42RF (N42RF)	fuselage, Rosemount 858 (± 0.5 m s^{-1})	PRT, deiced Rosemount 102A (± 0.6°C)	cooled mirror GE 1011 (± 0.6°C)	1 s
NOAA WP-3D N43RF (N43RF)	fuselage, Rosemount 858 (± 0.5 m s^{-1})	PRT, deiced Rosemount 102A (± 0.6°C)	cooled mirror GE 1011 (± 0.6°C)	1 s
NCAR Electra N308D (N308D)	radome (± 1.0 m s^{-1})	PRT, nondeiced Rosemount 102 (± 0.5°C)	cooled mirror GE 1011B (± 0.6°C)	1 s[d]
MRF UK C130 (C130)	nose boom vanes, Penny & Giles E23001 (± 0.4 m s^{-1})	PRT, nondeiced Rosemount 102AL (± 0.3°C)	cooled mirror GE 1011B (± 0.5°C)	1 s
FIAMS Cessna 340A (340A)	radome (± 0.5 m s^{-1})	thermocouple, Meteolab TP-4S (± 0.3°C)	cooled mirror Meteolab TP-4S (± 0.3°C)	1 s[e]
		Research Vessels (R/V)		
USN/UH *Moana Wave* (WAVE)	sonic anemometer, Gill Solent, at 15.0 m (± 0.2 m s^{-1})	Pt-100, Vaisala HMP-35 at 15.0 m (± 0.2°C)	CTF, Vaisala HMP-35 at 15.0 m (± 0.4 g kg^{-1})	~ 10 min
NSF/OSU *Wecoma* (WECM)	propeller & vane, R.M. Young at 20.8 m (± 0.2 m s^{-1})	shielded thermistor at 8.0 m (± 0.2°C)	Vaisala at 8.0 m (± 3%)	~ 1 min, 30 min
CSIRO *Franklin* (FRNK)	cup & vane, Rimco at 11.3 m (± 0.2 m s^{-1})	Bradley-aspirated psychrometer at 11.3 m (± 0.05°C)	Bradley-aspirated psychrometer at 11.3 m (± 0.15 g kg^{-1})	15 min
		Research Moorings		
NOAA/PMEL ATLAS (ATLS)	propeller & vane R.M. Young at 4.0 m (± 0.3 m s^{-1})	Rotronics, MP-100 at 3.0 m (± 0.2°C)	Rotronics, MP-100 at 3.0 m (± 4%)	60 min[f]
WHOI Mooring (IMET)	cup & vane, R.M. Young 12170C at 3.54 m (± 2.5%)	thermistor, Thermometrics at 2.78 m (± 0.1°C)	CTF, Vaisala Humicap at 2.74 m (± 0.1 g kg^{-1})	7.5 min

Abbreviations for each platform and estimated accuracies are in parentheses.
[a]PRT, platinum resistance thermometer.
[b]GE, General Eastern; CTF, capacitive thin film.
[c]SI, time interval between samples.
[d]Every 20th point selected from 20-Hz data.
[e]A 1-s boxcar-average from 20-Hz data.
[f]Hourly wind speed is a 6-min vector boxcar-average of 2-Hz wind data centered on the top of the hour; hourly air temperature and relative humidity are a 60-min boxcar average of data sampled every 10 min.

ences in aircraft mean measurements which are different from the findings of the present study.

The five boundary layer aircraft deployed in TOGA COARE were the two National Oceanic and Atmospheric Administration (NOAA) WP-3D Orions (N42RF and N43RF), the National Center of Atmospheric Research (NCAR) Electra N308D, the Meteorological Research Flight (MRF) C130, and the Flinders Institute for Atmospheric and Marine Sciences (FIAMS) Cessna 340A. In addition to these, two National Aeronautics and Space Administration (NASA) aircraft flew high-altitude missions that are not part of the present study. Main instrumentation and aircraft abbreviations are listed in Table 1. The respective flight facilities provide additional instrumentation and data processing details [*Lenschow and Spyers-Duran,* 1989; *Miller*

and Friesen, 1989; *Williams and Hacker,* 1993]; information is also available from previous investigations [*LeMone and Pennell,* 1980; *Serra et al.,* 1997; *Grant and Hignett,* 1998; *Khelif et al.,* 1999]. For the current study, all flight-facility-determined empirical adjustments have been removed so that "unadjusted" meteorological data are analyzed. This does not apply to the wind speed and direction comparison, where data are used as obtained from the respective data processing facility, which may have used maneuvers to calibrate the wind-measuring system [e.g., *Khelif et al.,* 1999]. It should be noted that the WP-3D data used in this study were processed at the University of California at Irvine (UCI), using techniques described by *Khelif et al.* [1999]. More information on obtaining the aircraft data is in Appendix A.

The importance of comparing data to assess measurement quality from multiaircraft experiments has been emphasized in previous studies. While most have compared fluxes and fluctuations of wind and scalars [*LeMone and Pennell,* 1980; *Nicholls et al.,* 1983; *MacPherson et al.,* 1992; *Dobosy et al.,* 1997], some have analyzed mean measurements [*Rockwood et al.,* 1977; *Nicholls,* 1983; *Lambert and Durand,* 1998]. Consequently, specific comparison flight patterns were flown throughout the COARE IOP as part of the boundary layer research flight missions. The meteorological measurements compared here are ambient temperature (T), dew point (T_d), specific humidity (q), barometric pressure (BP), static pressure measured at flight level (P_{sm}), wind speed (WS), and wind direction (WD). The WD convention is the meteorological one, the direction the wind is coming from. Aircraft radar altitude (Hr) data are also compared.

As outlined by *Fairall et al.* [1996b], the COARE goal of achieving a bulk parameterization accuracy of ±6-7 W m^{-2} for the sum of the latent and sensible heat fluxes requires that systematic measurement errors be less than ±0.2°C for T, ±0.2 g kg^{-1} for q, ±0.2 m s^{-1} for WS, and ±0.2°C for the sea surface temperature. Sea surface temperatures are not compared in this study but are compared in a similar study by S.P. Burns et al. (Comparisons of aircraft, ship, and buoy radiation and SST measurements from TOGA COARE, submitted to *Journal of Geophysical Research,* 1999). When laboratory calibrations are applied to the recorded data, the resulting aircraft-aircraft comparisons often have differences in excess of the above desired accuracies. The sources of these discrepancies are generally unknown; factors such as local flow distortion may be a source of error but are hard to quantify; therefore empirical corrections (in the form of a constant offset) can be used to adjust for the differences. Flight facilities sometimes account for such errors on the basis of aircraft maneuvers, tower fly bys, etc. These are usually determined in single-aircraft test flights but not under the conditions of a particular field experiment. An attempt is made here to determine differences in the aircraft data under a variety of actual tropical COARE conditions and to develop rational corrections which improve the overall measurement accuracies.

After a determination of the aircraft-relative empirical corrections from the wingtip-to-wingtip comparisons, these data were compared to corresponding measurements from ships and buoys in the intensive flux array (IFA). The TOGA COARE bulk flux algorithm [*Fairall et al.,* 1996b] was used to adjust for height differences between the aircraft (15 to 100 m) and the surface platforms (3 to 21 m). Data from the following surface platforms were considered: (1) the Woods Hole Oceanographic Institution (WHOI) mooring, which had three different instrumentation packages (two improved meteorological (IMET) instruments and a vector-averaging wind recorder (VAWR) [*Weller and Anderson,* 1996]); (2) one of the NOAA/Pacific Marine Environmental Laboratory (PMEL) Autonomous Temperature Line Acquisition System (ATLAS) moorings (see *Cronin and McPhaden* [1997] for more information on the Tropical Ocean Atmosphere (TAO) buoy array during COARE); (3) the Australian Commonwealth Scientific and Industrial Research Organisation (CSIRO) R/V *Franklin*; (4) the U.S. Navy owned and University of Hawaii operated R/V *Moana Wave*; and (5) the National Science Foundation (NSF) owned and Oregon State University (OSU) College of Oceanic and Atmospheric Sciences (COAS) operated R/V *Wecoma.* A summary of the surface platform instrumentation is given in Table 1.

To allow judgment of the effects of the aircraft empirical corrections, all low-altitude data (< 100 m) collected by the five aircraft over the IOP were combined and compared with the ship and buoy data from similar time periods. These comparisons also revealed the fair weather variability of important air-sea parameters, which were sampled by aircraft missions that contained low-level runs.

2. Aircraft-Aircraft Comparisons

Within this section the aircraft "wingtip-to-wingtip" comparisons (periods when two or three aircraft were flying side by side of each other on a constant heading and elevation) are used to find relative empirical corrections to the aircraft data which create a more consistent aircraft data set. The absolute value of the corrections were partly based on consideration of aircraft-surface comparisons presented later.

To obtain a broader perspective than the wingtip-to-wingtip comparisons, all the low-level data collected by each aircraft will also be compared. These comparisons reveal discrepancies between the aircraft within the context of the overall range of the measured data and provide deeper insight into the effect of the proposed empirical corrections on the measured data.

2.1. Wingtip-to-Wingtip Comparisons

An aircraft wingtip-to-wingtip comparison period was defined as the period when two or three aircraft were

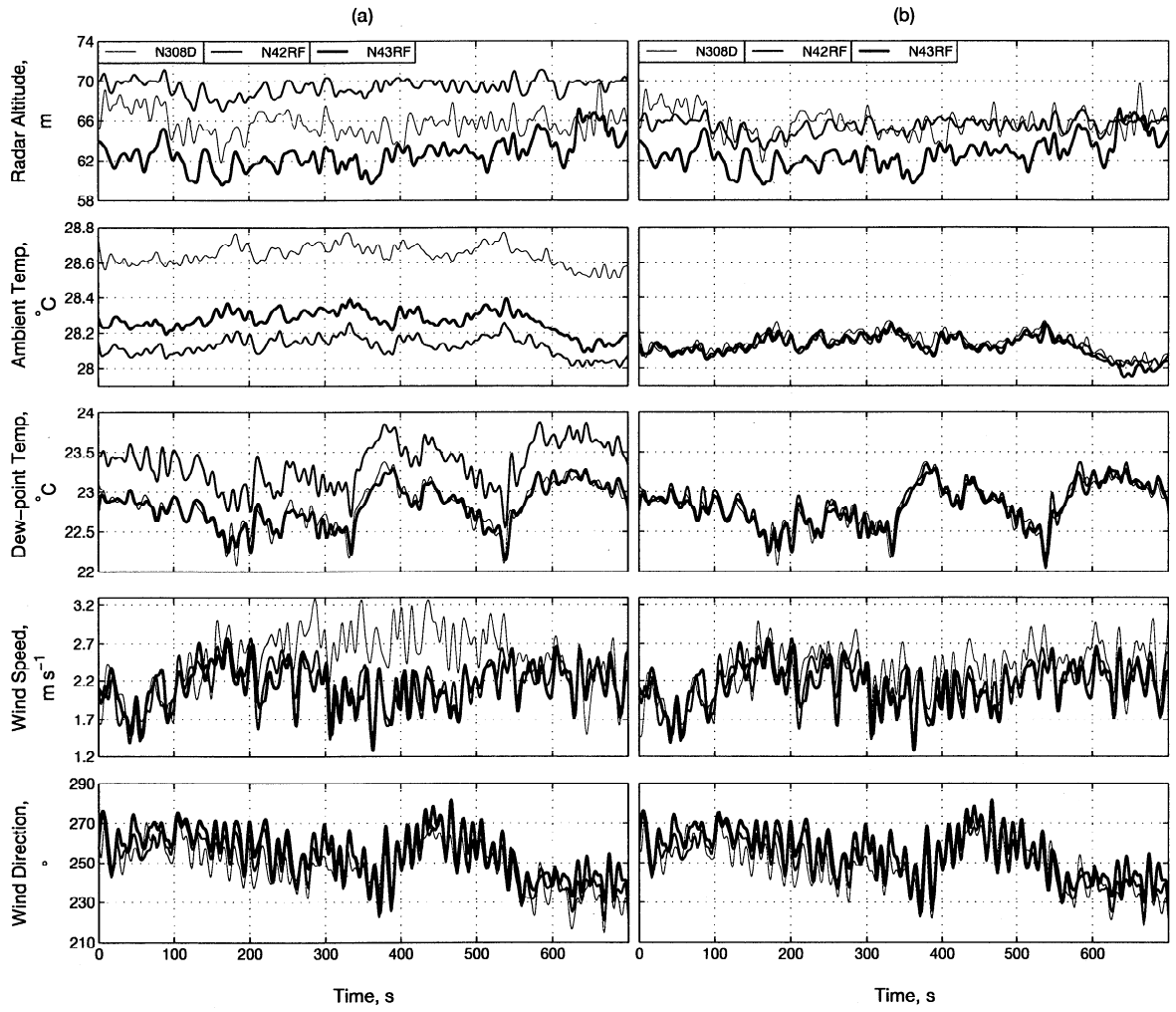

Figure 1. Time series from a three-aircraft wingtip-to-wingtip comparison leg (921128, 35400 - 40540 UTC) of (a) uncorrected (N308D winds are NCAR-processed) and (b) empirically corrected (N308D winds are Raymond-processed) data. See text for an explanation of Raymond-processed wind data. To emphasize mean structure, these data are low-pass-filtered at 0.1 Hz.

flying below 250 m on a constant heading with small lateral (< 100 m), longitudinal (< 100 m), and vertical (< 10 m) separations between the aircraft. The close formation did not appear to cause aerodynamic interference errors except for the mean vertical winds, which are not compared here (these are compared by *Khelif et al.* [1999]). There were a total of 38 comparison periods (see section A2) which ranged from 30 s (≈ 3 km track) to over 20 min (≈ 120 km) and satisfied the above conditions. Of these, 23 occurred as a two-aircraft combination of N308D, N42RF, or N43RF, and 6 were three-aircraft comparisons. The remaining 9 comparisons were either C130 versus N42RF, or 340A versus N308D. Details of the comparisons are in Appendix A.

Comparison time periods were selected according to the above criteria, and typical time series of radar altitude, ambient temperature, dew point, wind speed, and wind direction from a three-aircraft (N308D, N42RF, and N43RF) comparison on 921128 (this is the mission ID based on aircraft takeoff UTC date: YYMMDD) are shown in Figure 1, column a. (These data were lightly filtered to emphasize offsets and trends; and the difference between NCAR-processed and Raymond-processed wind data is explained in section 2.1.5.) The systematic errors in most of the variables do not meet the previously mentioned COARE goals outlined by *Fairall et al.* [1996b]. The same time series with empirical corrections applied are shown in Figure 1, column b. The method used to determine these corrections considered all comparison time periods throughout the COARE IOP and is described in detail in this paper.

Comparison results are based on 100-s (≈ 10 km) means of the aircraft data, unless otherwise specified. Scatter plots and box-and-whisker plots are used to display the comparison results. (A box plot [e.g., *Hoaglin et al.*, 1983] displays data in quartiles where the "box" indicates the interquartile range (iqr) over which the

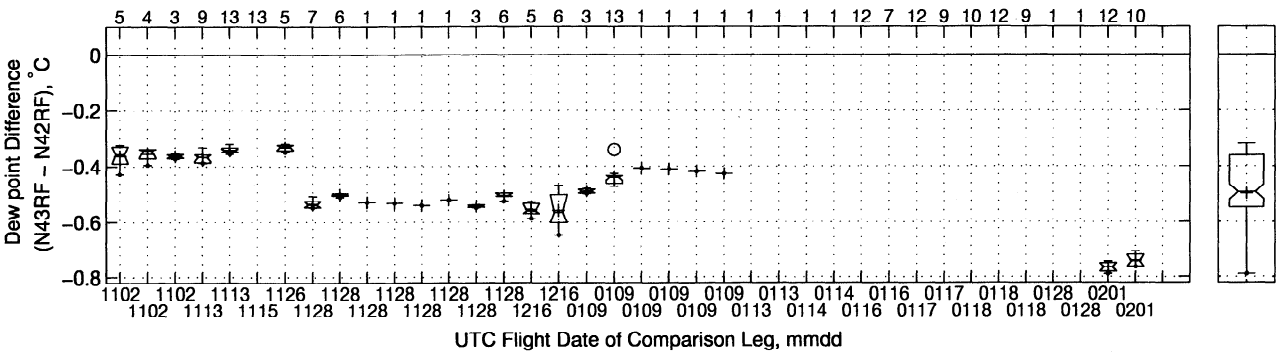

Figure 2. Box plots of the mean difference between raw dew point measured on N42RF and N43RF. Each box plot represents a single intercomparison leg with the number of 100-s mean values shown above. To the far right is the overall-mean-difference box plot. Legs without a box plot indicate that N42RF and N43RF did not directly compare on that particular leg. See text for description of box plots.

middle 50% of the data are distributed, the lowest 25% of the data are between the lower end of the box and the lowest whisker endpoint, and the upper 25% are between the top of the box and the upper whisker. The line through the box shows the median. The mean is designated by a "plus" and outliers (defined as points that are greater than 1.5 (iqr) away from the edge of the box) by a "circle".)

The box plot was used to graphically display and compare mean differences between measured variables. It is a robust way to display the mean difference between measurements from two sensors, giving information about how the mean difference varied throughout a comparison leg, as well as the simple mean difference for the entire leg. For a given leg, a small spread in the box plot of the mean difference between two different sensors indicates that measurement differences between these two sensors remained fairly constant throughout the leg. If these differences persisted and remained constant over many different legs, then "systematic" errors were present in one or both of these sensors. To explore how the mean difference between two sensors varied throughout the IOP, a chronological series of box plots was generated which revealed any changes in agreement over time between these instruments. An example is shown in Figure 2 where the mean difference in dew point between N42RF and N43RF is displayed. While the overall box plot (on the far right) gives a rough estimate of agreement between the two instruments, it is clear, by looking at the individual leg box plots, that the agreement between the instruments varied throughout the IOP. By comparing data from redundant sensors and data between the aircraft, date-dependent empirical corrections for certain sensors were deemed necessary.

The 340A-N308D comparison periods were selected using a slightly different approach than that used for the other aircraft due to the airspeed difference between the two aircraft. The slower 340A aircraft (airspeed$\approx$ 65 m s^{-1}) was overtaken by N308D (airspeed$\approx$ 105 m s^{-1}), and a 30-s period around the passing point was used as the comparison time interval.

As shown in Table 2, only five different combinations of the five aircraft flew together (C130 flew only with N42RF, and 340A flew only with N308D). For this reason, N42RF and N308D are considered the "refer-

Table 2. Number of Aircraft Wingtip-to-Wingtip and Aircraft-to-Surface Platforms TOGA COARE Comparison Periods

Wingtip-to-Wingtip		Aircraft-to-Surface Platform						
Combinations	No.[a]	Aircraft	IMET No.[b]	ATLS No.[b]	WECM No.[b]	WAVE No.[b]	FRNK No[b]	Symbol Legend
N43RF, N42RF[c]	118	N42RF	36	6	8	26	6	triangle
C130, N42RF[c]	34	C130	4	2	0	0	2	solid circle
N308D, N42RF[c]	59	N308D	15	8	5	11	30	square
N43RF, N308D[c]	71	N43RF	21	4	6	23	10	inverted triangle
340A, N308D[c]	6	340A	5	2	6	3	28	open circle

Column 9 is the symbol legend to be used in Figures 2-5, 8-13, and 15-18.

[a]Number of 100-s mean aircraft-to-aircraft comparison points from the 38 aircraft wingtip-to-wingtip comparisons.

[b]Number of aircraft runs over surface platforms.

[c]Aircraft designated as the "reference" during wingtip-to-wingtip comparisons.

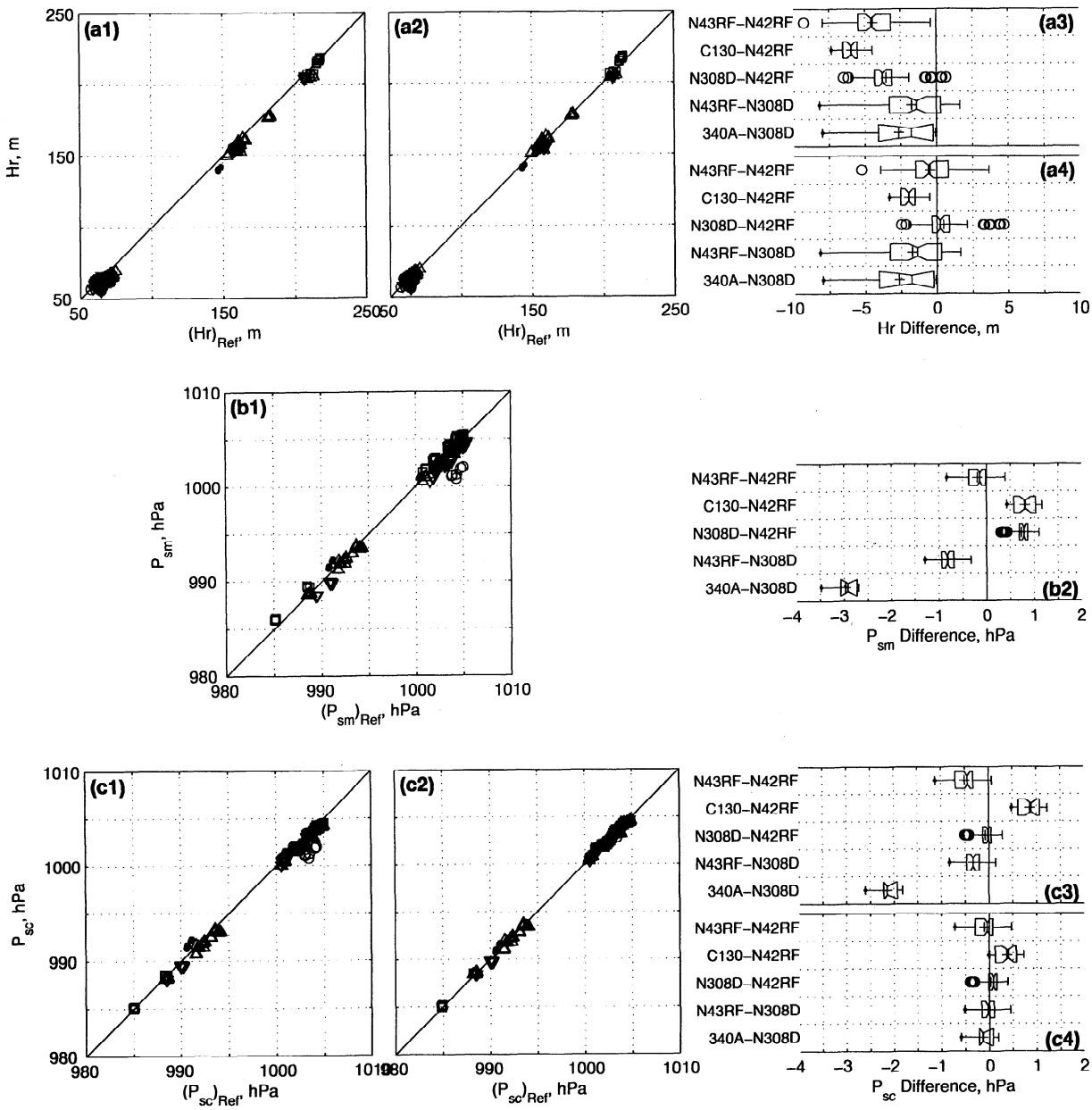

Figure 3. Scatterplots and box plots comparing (a1-a4) radar altitude Hr, (b1-b2) raw static pressure P_{sm}, and (c1-c4) static pressure corrected for static pressure defect P_{sc} with symbols as in Table 2. Each scatterplot has a corresponding box plot which shows the mean data differences. For each row, the left-hand scatterplot is associated with the top box plot. The combinations are raw-measured data (a1/a3,b1/b2), data corrected for static pressure defect (c1/c3), and empirically adjusted data (a2/a4,c2/c4).

ence" aircraft against which the other aircraft are compared. In Table 2 the various aircraft combinations and the number of 100-s segments for each combination are shown.

Before proceeding to the comparison of calculated winds, the state variables of ambient temperature, dew point, radar altitude, and static pressure are considered. Of these, dew point and radar altitude are measured directly, and the accuracy is set solely by the instruments. Ambient temperature and defect-corrected static pressure (explained below) are calculated on the basis of other measured variables.

2.1.1. Radar altitude. Geometric altitude was measured with Gould APN-232 radar altimeters on N42RF and N43RF, a Collins (model ALT 55B) radio altimeter on N308D, a Honeywell radar altimeter on the C130, and a King KRA-10A radar altimeter on the 340A. There was also a Stewart-Warner APN-159 radar altimeter on each of the two WP-3Ds but the signals from these instruments interfered with each other during the comparison legs so they were disabled. The scatter plot (Figure 3a1) and corresponding box plot (Figure 3a3) show that raw Hr measured by N42RF was consistently higher than that of any aircraft fly-

ing alongside. As further evidence that Hr on N42RF was biased high, data from the N42RF, N43RF, and N308D aircraft on the ground before takeoff and after landing were compared. Data from N42RF were about 4 m higher than those of the other aircraft, so Hr data on N42RF were reduced by that amount. The box plot of the empirically adjusted data (Figure 3a4) shows the improvement in the N43RF, C130, and N308D versus N42RF comparisons.

2.1.2. Static pressure. Static pressure is normally measured from the aircraft manufacturer's fuselage static ports that are used for avionics, or from the static side of research Pitot-static probes that are placed on special booms. Since the flow around the aircraft alters the static pressure field, a determination must be made of the difference between the true static pressure away from the aircraft in the same horizontal plane and the pressure measured: this difference is called the static pressure defect. For the WP-3Ds and Electra this was determined before COARE, using the trailing-cone technique [*Brown,* 1988]. The defect typically depends on airspeed, and the correction technique used for the WP-3D data is described by *Khelif et al.* [1999]. The comparison results of raw static pressure (Figures 3b1 and 3b2) clearly show that N308D data are greater by about 0.8 hPa than those measured by N42RF and N43RF. Figure 3c3 is the corresponding box plot of these data after correction for the static pressure defect. There were no static pressure defect determinations for 340A and C130, which is why there are large differences in comparisons involving these two aircraft. When comparing Figures 3b2 and 3c3, it is apparent that while the defect-corrected static pressure between N42RF and N308D are now in reasonable agreement, the difference between N43RF and N42RF has actually increased by almost 0.3 hPa. This is evidence that the static pressure defect correction is slightly imperfect on one or both of these aircraft. Since defect-corrected N308D and N42RF pressure data were in reasonable agreement, we have applied constant corrections (in addition to any static pressure defect correction); this will bring all the aircraft into agreement with N308D, which has had many trailing cone tests performed on it. The values of these constant empirical corrections are given in Table 3. The final box plot (Figure 3c4) compares these data after applying both the defect correction (which depends on airspeed) and the constant empirical correction. The agreement between all aircraft is now less than ±0.75 hPa for all level comparison legs. Some of the difference in the N42RF-C130 comparison static pressure data can be attributed to differences in aircraft elevation.

2.1.3. Dew-point temperature. All five aircraft used chilled-mirror hygrometers for slow-response measurement of dew-point temperature (Table 1). From Figure 4a3 (and Figure 1a) it is evident that the N42RF General Eastern hygrometer dew-point temperatures were biased high by at least 0.4°C. In addition to this mean difference it appears that some February flights had even greater deviations. It was thought that redundant sensors on the aircraft would be helpful in deciding which sensor measured the more accurate T_d, but the two sensors on N42RF both measured a higher T_d than the three sensors on N43RF. The N308D General Eastern data were in agreement with the N43RF data, while the N308D EG&G data (a second dewpointer on N308D whose output contained severe oscillations) agreed better with the N42RF data. Comparisons between N42RF and C130 showed the N42RF dew-point data to be too high, while 340A and N308D comparisons showed the N308D General Eastern data to be fairly accurate.

After taking into consideration the surface platform data, we decreased the N42RF data (see Table 3 and Figure 5a) and increased the C130 data to be consistent with that of N43RF and N308D. This reduced the spread in the dew-point comparison from nearly 0.8°C to less than 0.2°C (compare Figures 4a3 and 4a4). A comparison of specific humidity is included since dew point was not part of the 340A public-domain data set. The comparison for q is essentially identical to the T_d comparison (compare Figures 4a1-a4 with 4b1-b4), and based on the numerous 340A comparisons with *Franklin*

Table 3. Empirical Corrections to Aircraft Mean Measurements

	Formula: $X_{adjusted} = X_{original}$ + *Empirical Correction*				
Parameter	C130	N308D	340A	N42RF	N43RF
Hr, m	0	0	0	-4	0
P_{sc},[a] hPa	-0.6	0	2.0	-0.1	0.3
T_d, °C	0.25	0 to 0.1	-	-1.4 to -0.35	-0.1 to 0
q, g kg^{-1}	-	-	-0.1	-	-
T, °C	-0.55	-0.6 to 0	0	0 (f2)	-0.15 (f2)

Values shown are for radar altitude Hr, static pressure P_{sc}, dew point T_d, specific humidity q, and ambient temperature T. Date-dependent corrections show the minimum and maximum correction values; see Figure 5 for more information. WP-3D temperature corrections apply to "f2" sensor data only.

[a]N42RF and N43RF values shown are in addition to the static pressure defect correction (see text for details).

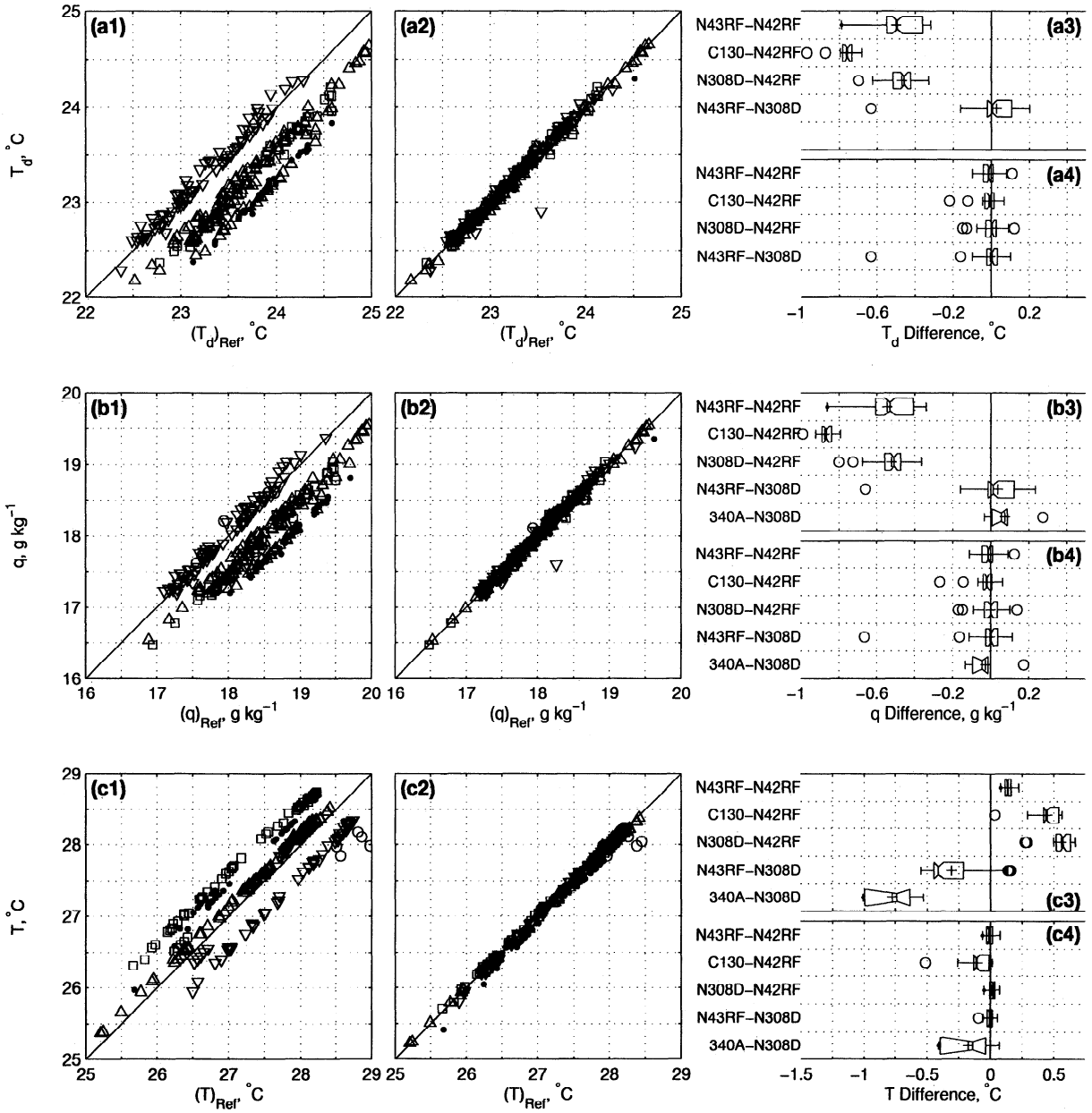

Figure 4. Same as Figure 3 except for (a1-a4) dew-point temperature T_d, (b1-b4) specific humidity q, and (c1-c4) ambient temperature T.

(discussed in more detail in Section 3), a small adjustment to the 340A specific humidity data (decreased by 0.1 g kg^{-1}) results in reasonable agreement between N308D and 340A data.

2.1.4. Ambient temperature. Temperature sensors on aircraft measure recovery temperatures, which are used to obtain ambient temperature through the compressible flow equations and knowledge of the recovery factor [*Liepmann and Roshko,* 1957] which depends on the sensing element and housing. For the WP-3D aircraft the small Mach-number dependence of the Rosemount probe recovery factor was used in the data reduction [*Khelif et al.,* 1999]. Constant recovery factors were used for N308D, 340A, and C130.

Each WP-3D aircraft carried two slow-response Rosemount temperature sensors (distinguished as "f1" and "f2" by the NOAA Aircraft Operations Center (AOC)). Data from these sensors were compared, and then, based on sensor performance throughout the IOP, one was chosen as the reference. For example, N43RF data from the "f1" sensor were consistently ~ 0.2°C greater than those from the "f2" sensor. To be consistent from one flight to the next, either the same temperature probe must be used or the difference between these data accounted for. For the current study, the "f2" probe on both WP-3Ds was used as reference for all flights and any offsets mentioned herein should be applied to "f2" sensor data only. The WP-3D "f2" sensor data

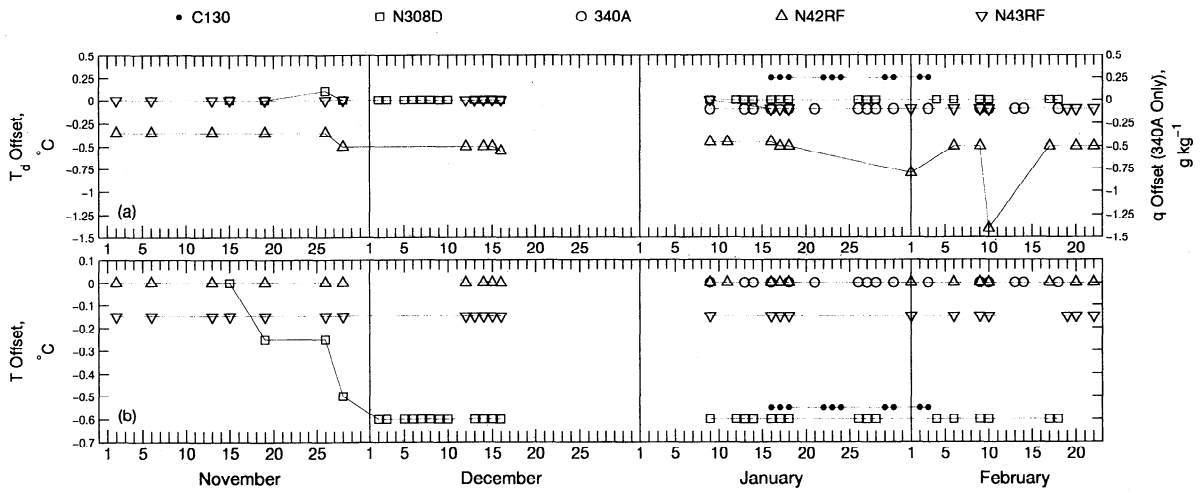

Figure 5. Empirical corrections to aircraft data for (a) dewpoint T_d (340A correction is on specific humidity q), and (b) ambient temperature T. Use legend to identify aircraft. Symbols specify the mission flight date.

were brought into agreement by applying the constant N43RF offset given in Table 3.

All aircraft mean T differences were within 0.6°C as shown in Figures 4c1 and 4c3. The differences between the various aircraft were fairly constant throughout the IOP except for N308D, which showed inconsistent data differences for flights prior to 921202 for the nondeiced Rosemount 102 sensor (ATB) data. The reason for this inconsistency was not determined, but comparison to the N308D wingtip temperature sensor suggested that ATB data collected after 921202 should be decreased by 0.6°C, while those collected prior to 921202 should have a flight-dependent offset, as shown in Figure 5b.

2.1.5. Earth-referenced winds. The horizontal winds calculated from the COARE boundary layer aircraft used radome, fuselage, or nose boom wind-measuring systems (see Table 1). For the WP-3D aircraft the winds calculated from the fuselage system were deemed more consistent and reliable than the radome data [*Khelif et al.*, 1999] and therefore were used in the comparisons. All aircraft horizontal winds are calculated using Inertial Navigation System (INS) horizontal ground speed data improved with Global Positioning System (GPS) data. The N308D and WP-3D wind-calculation techniques are detailed by *Lenschow and Spyers-Duran* [1989] (no information on use of GPS) and *Khelif et al.* [1999], respectively. For WP-3D, N308D, and 340A data the true airspeed was calculated using moist air properties.

With the exception of the WP-3Ds, none of the previously mentioned empirical corrections to T, T_d, and P_{sc} were applied prior to calculation of the wind components compared in this section. The wind data were taken "as is" from the respective aircraft data processing center or source. Tests with WP-3D data revealed that the effect of varying T and T_d (by the same approximate magnitude as the empirical corrections) on the calculated horizontal winds was small (less than 0.1 m s^{-1}) and therefore deemed insignificant.

After the initial N308D winds were processed by NCAR, David Raymond (Department of Physics, New Mexico Institute of Mining and Technology, Socorro) recalculated them using a different method of blending the GPS and INS ground speed data (see Appendix A for details on obtaining these data). The NCAR GPS-corrected winds were considered "experimental" by NCAR, and therefore details of the GPS-INS blending method are not readily available. Both NCAR- and Raymond-processed winds are compared with the other aircraft in the box plots of Figure 6. In general, the Raymond-processed winds agreed slightly better with the other aircraft than those processed by NCAR; therefore they are used throughout this paper. A comparison of time series from these two data sets (Figure 1) exemplifies the differences. Overall, wind speed and wind direction comparisons were reasonable, with no bias toward any particular aircraft.

2.2. Ensemble Comparisons

In addition to the wingtip-to-wingtip comparisons it is useful to examine the ensemble of all low-level aircraft data regardless of spatial proximity to each other. With the large amount of data collected, biases in the aircraft data may be revealed, and the effect of the empirical corrections can be evaluated. The 1-Hz aircraft data used are restricted to the latitudes, longitudes, and altitudes shown by the frequency distributions in Figure 7 (the ship frequency distributions in this figure will be referred to later).

Figure 8 shows the frequency distributions of aircraft raw data (T, q, WS, and WD), corrected-with-offsets data (T and q), and data adjusted to 10 m with the COARE bulk algorithm (use of the COARE bulk algo-

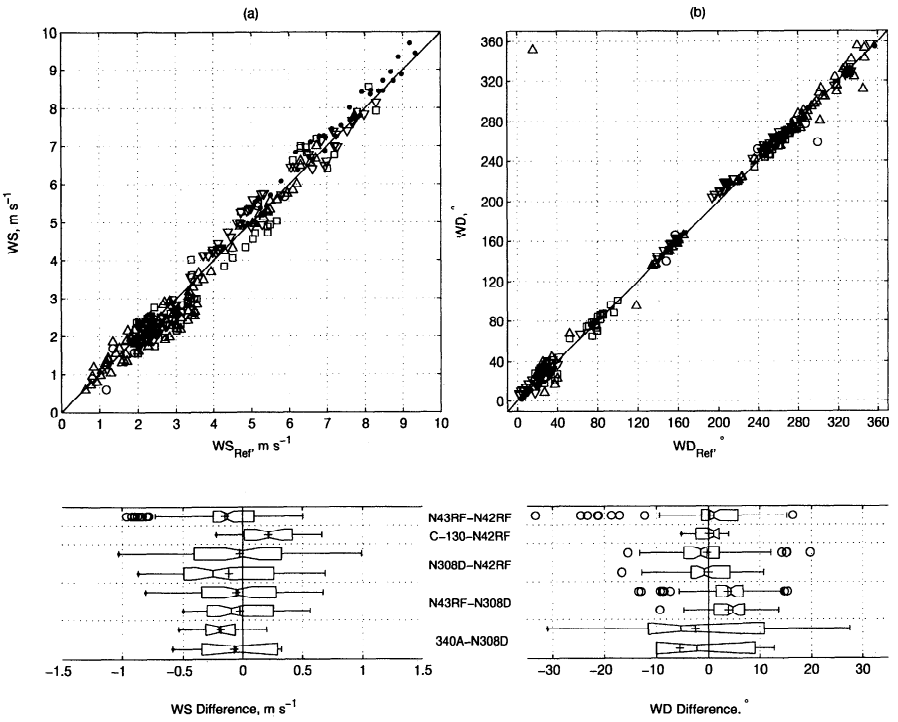

Figure 6. Scatterplots and box plots comparing (a) wind speed WS and (b) wind direction WD using symbols as in Table 2. Mean data differences measured on two different aircraft are displayed as box plots (middle text indicates aircraft pair being compared). For the aircraft combinations which involved N308D there are two box plots shown; the top box plot of each pair uses N308D NCAR-processed wind vector data, and the bottom box plot uses N308D Raymond-processed wind vector data. (Raymond data are used in the scatterplot.)

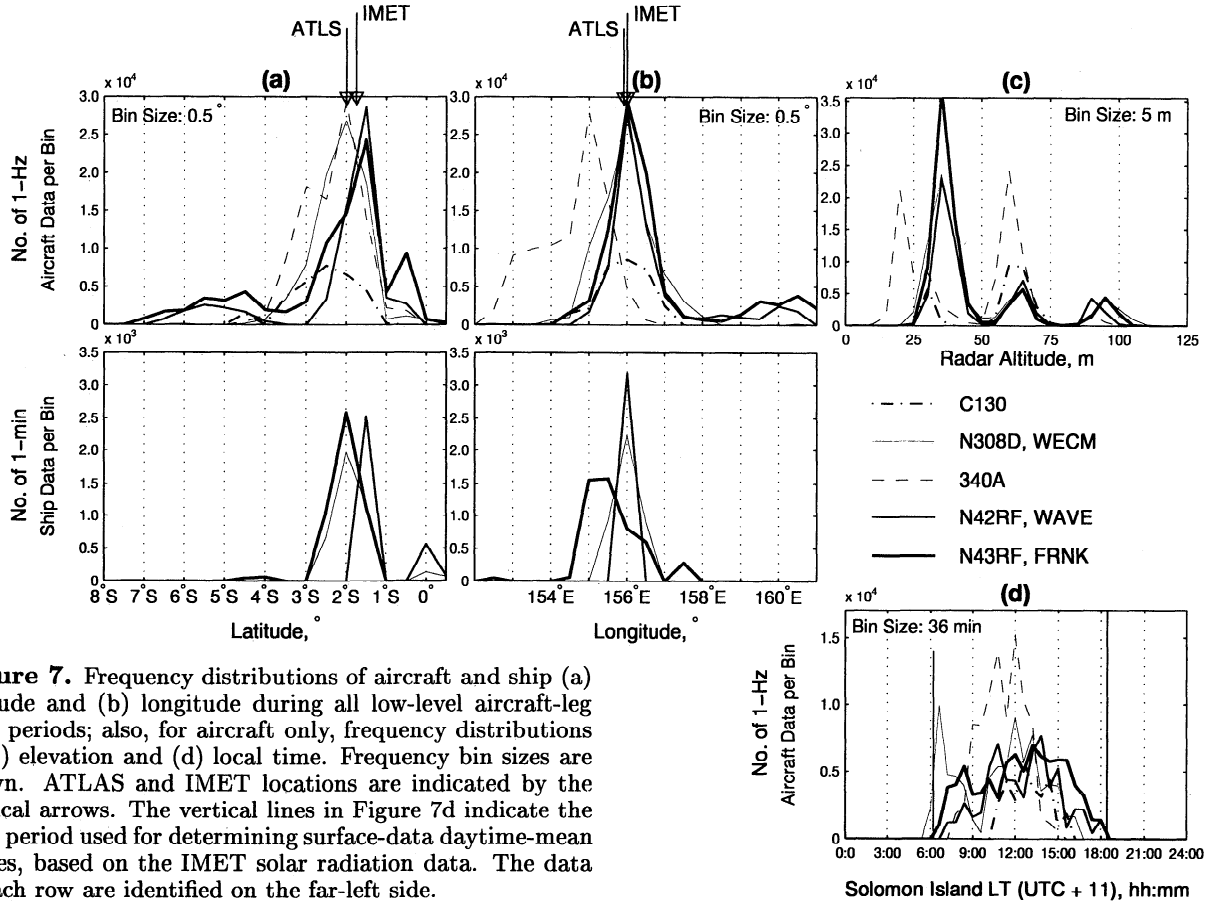

Figure 7. Frequency distributions of aircraft and ship (a) latitude and (b) longitude during all low-level aircraft-leg time periods; also, for aircraft only, frequency distributions of (c) elevation and (d) local time. Frequency bin sizes are shown. ATLAS and IMET locations are indicated by the vertical arrows. The vertical lines in Figure 7d indicate the time period used for determining surface-data daytime-mean values, based on the IMET solar radiation data. The data of each row are identified on the far-left side.

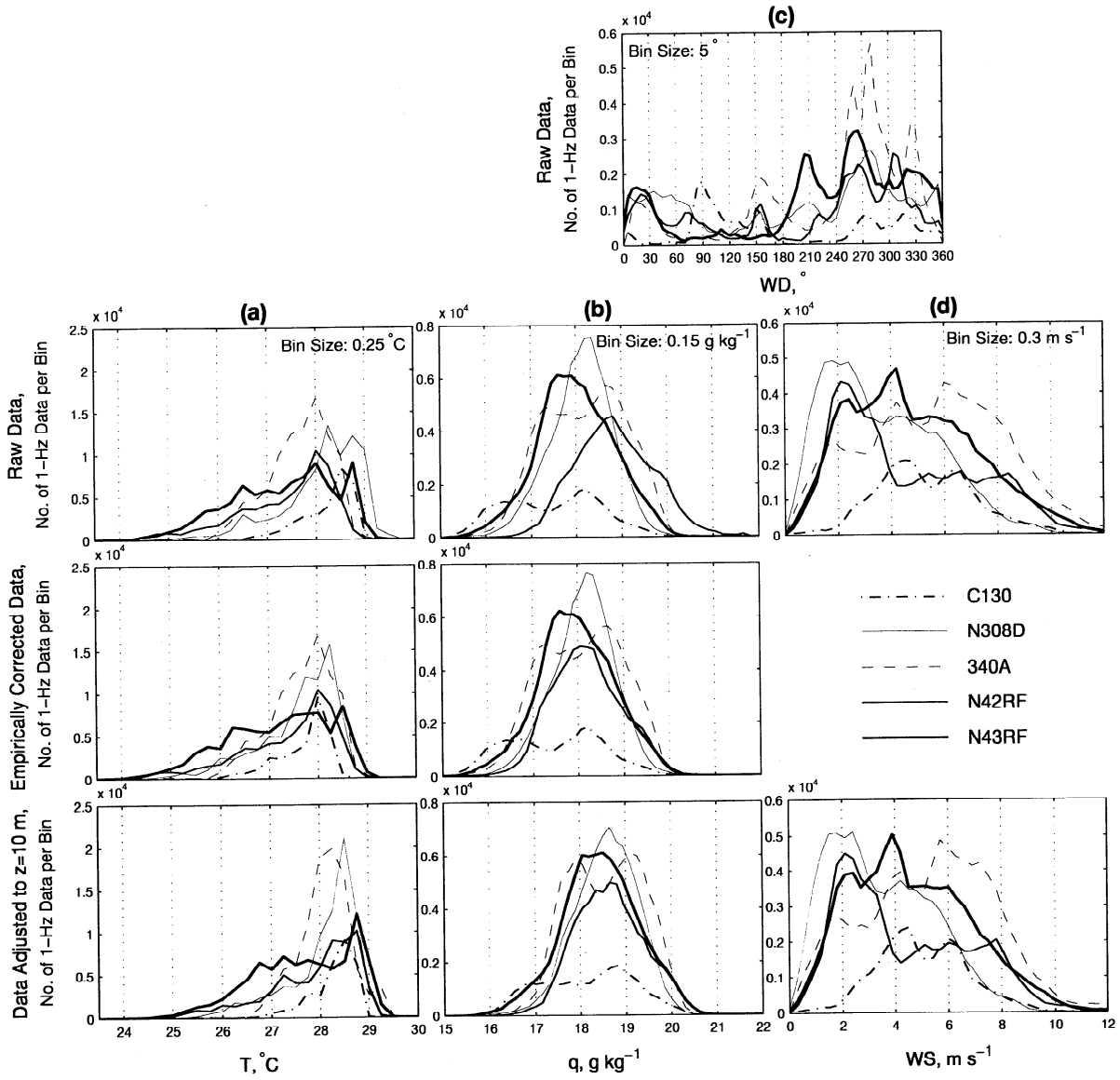

Figure 8. Frequency distributions of (a) ambient temperature T, (b) specific humidity q, (c) wind direction WD, and (d) wind speed WS for C130, N308D, 340A, N42RF, and N43RF low-level-run 1-Hz data. Bin sizes are shown in top panels. The data of each row are identified on the far-left side.

rithm with aircraft data is discussed more in the next section). The raw ambient temperature frequency distribution from N308D shows greater T values than those measured by the other aircraft, which is consistent with the dedicated formation comparisons of section 2.1.4. Agreement improves by applying the N308D empirical correction (Figure 8, column a). The frequency distributions for specific humidity show general agreement for the raw data and are perhaps brought closer by the empirical corrections and adjustment to 10 m. The 340A q distribution has two peaks due to the two favored elevations it flew (25 and 40 m; see Figure 7). The many low C130 q values ($\sim$ 16 g kg^{-1}, Figure 8b) are traced to missions 930123 and 930124, when IMET and *Franklin* measured the lowest q values throughout the IOP, and C130 was the only aircraft flying (this can be seen in figures of section 4).

The individual wind speed frequency distributions are more varied, reflecting different conditions sampled by the individual aircraft; e.g., N308D was used in many flights with low-wind, suppressed conditions, while the C130 flew in primarily moderate wind situations. Wind direction agreement is reasonable, with most data showing the preferred westerlies.

3. Aircraft-Buoy and Aircraft-Ship Comparisons

In addition to aircraft-aircraft comparisons, aircraft-buoy and aircraft-ship overflights were also performed

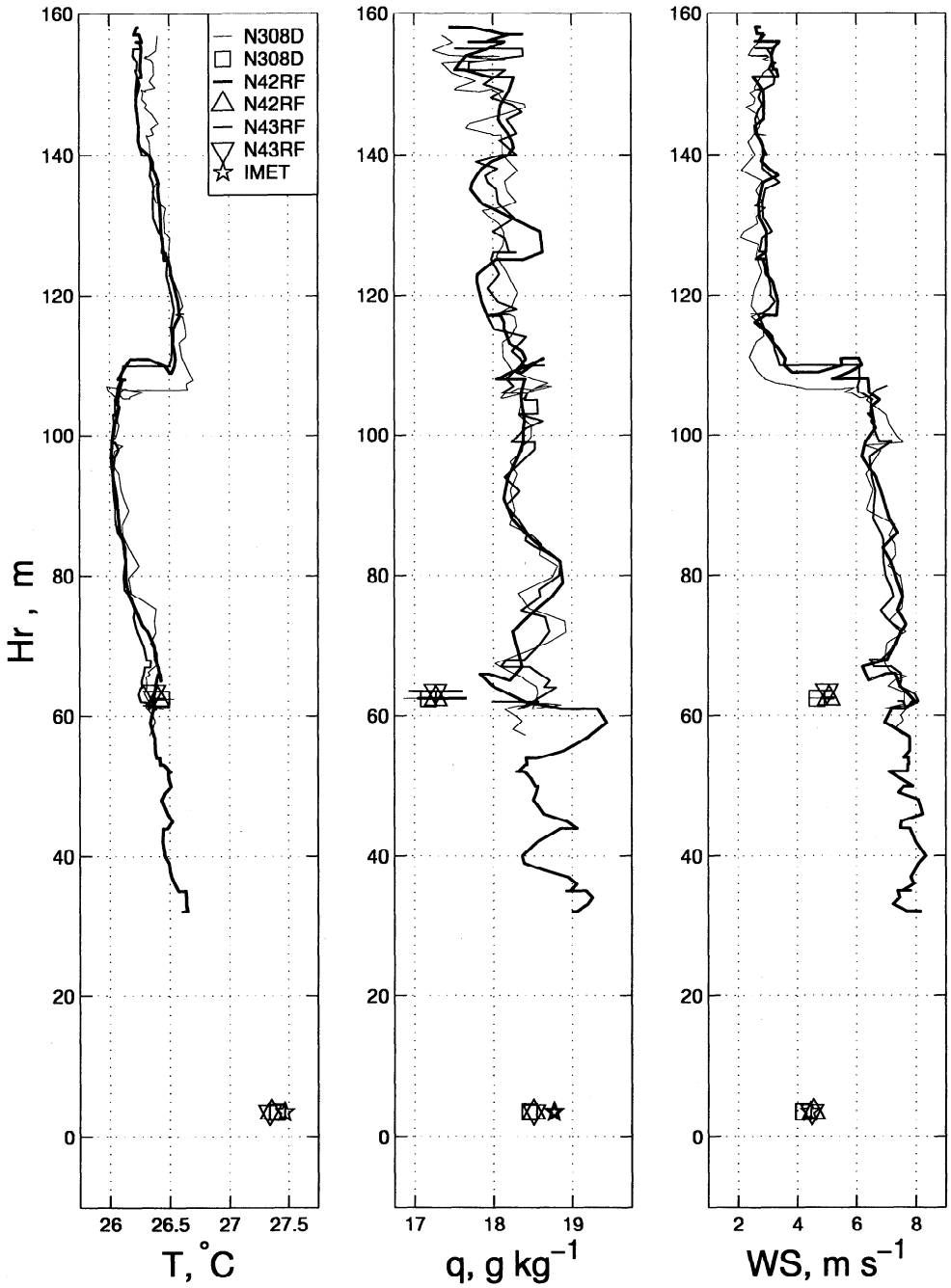

Figure 9. Soundings and level-run means over IMET from the two WP-3Ds and N308D from 921126. The lines across aircraft data symbols at aircraft height indicate the data range over the 20-s averaging period. The aircraft-IMET lateral separation was ~ 5.6 km, and the sounding was performed at end of the overflight leg 85 km away from IMET. Data from the aircraft are adjusted to IMET-sensor heights using the COARE bulk flux algorithm.

to further validate the interaircraft biases determined above. Such comparisons have been used to check data quality in past experiments by *Stuart et al.* [1981], *Nicholls* [1983], *Friehe et al.* [1984], and *Beardsley et al.* [1996].

Since the aircraft flight levels used in this study ranged between 15 and 100 m and most of the surface sensors were between 3 m (buoys) and 8-20 m (ships), the height differences in the surface layer gradients can have a large effect on the comparisons. The usual solution is to assume that the low-level aircraft data are in the constant flux surface layer and use the flux-profile relationships [e.g., *Businger et al.*, 1971] to extrapolate the aircraft data down or the ship/buoy data up. We used the height adjustment flux-profile procedure developed from the COARE data by *Fairall et al.* [1996b] to adjust data from aircraft level to the surface-platform sensor height.

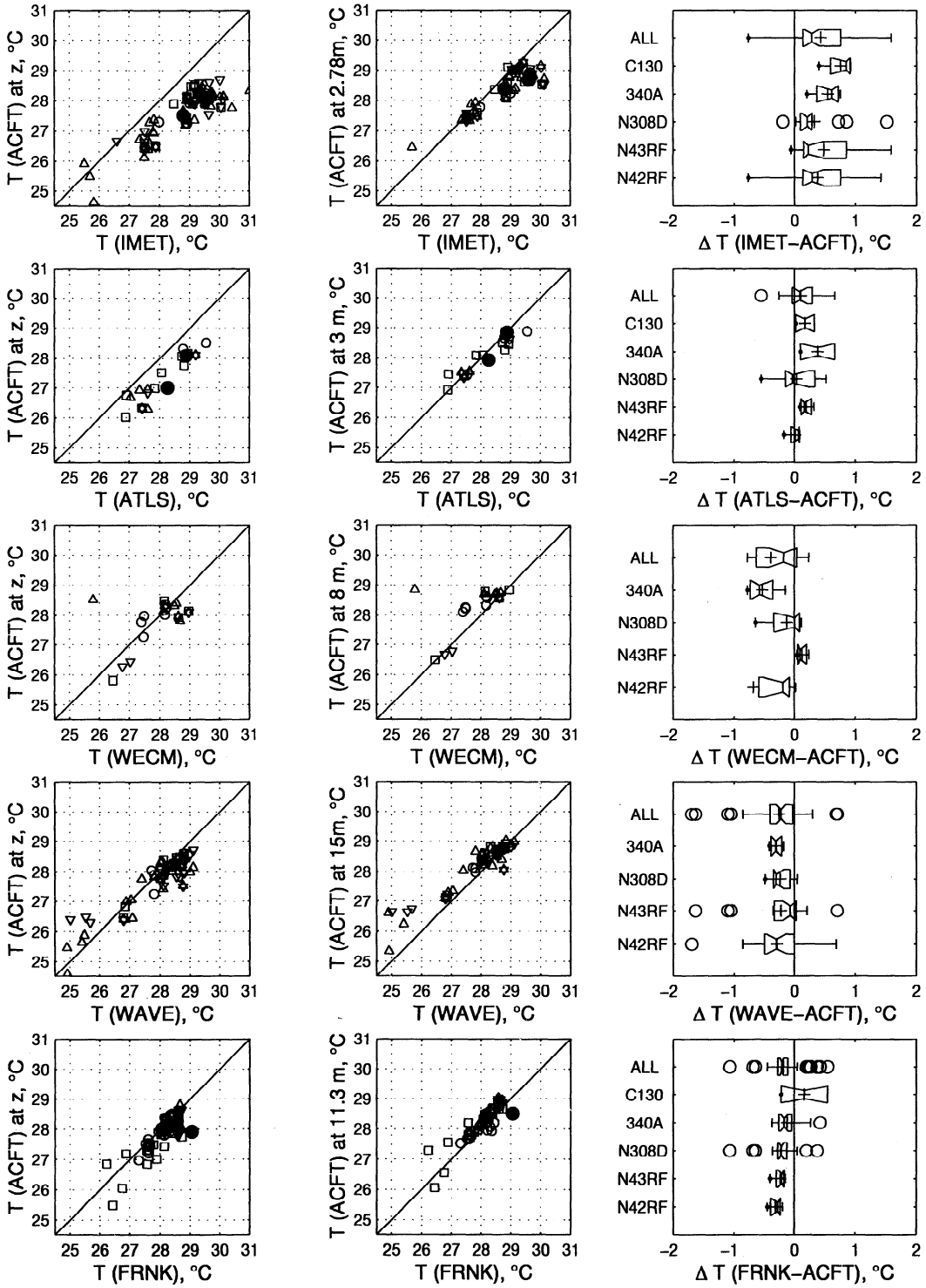

Figure 10. Comparison of ambient temperature T measured from aircraft and T measured by IMET (top row), ATLAS (row 2), *Wecoma* (row 3), *Moana Wave* (row 4) and *Franklin* (bottom row). In the scatterplots aircraft data are at flight level (left) and adjusted to the height of the surface-platform instrument (right). The solid line is the one-to-one line. Box plots show differences between the height-adjusted aircraft measurements and the surface-platform measurements. Refer to Table 2 for key to symbols. The IMET data shown are uncorrected for solar heating errors.

Sample vertical profiles of aircraft soundings, together with IMET data, aircraft overflight data, and the height-adjusted aircraft overflight data, are shown in Figure 9. While it is difficult to reach an overall conclusion based on a few of such samples, the flux-profile height extrapolations from aircraft levels of 30 and 60 m are reasonable, especially for temperature. For all of the comparison overflights we chose to use the flux-profile method for aircraft heights up to 100 m. There was no adjustment of wind direction. An important input

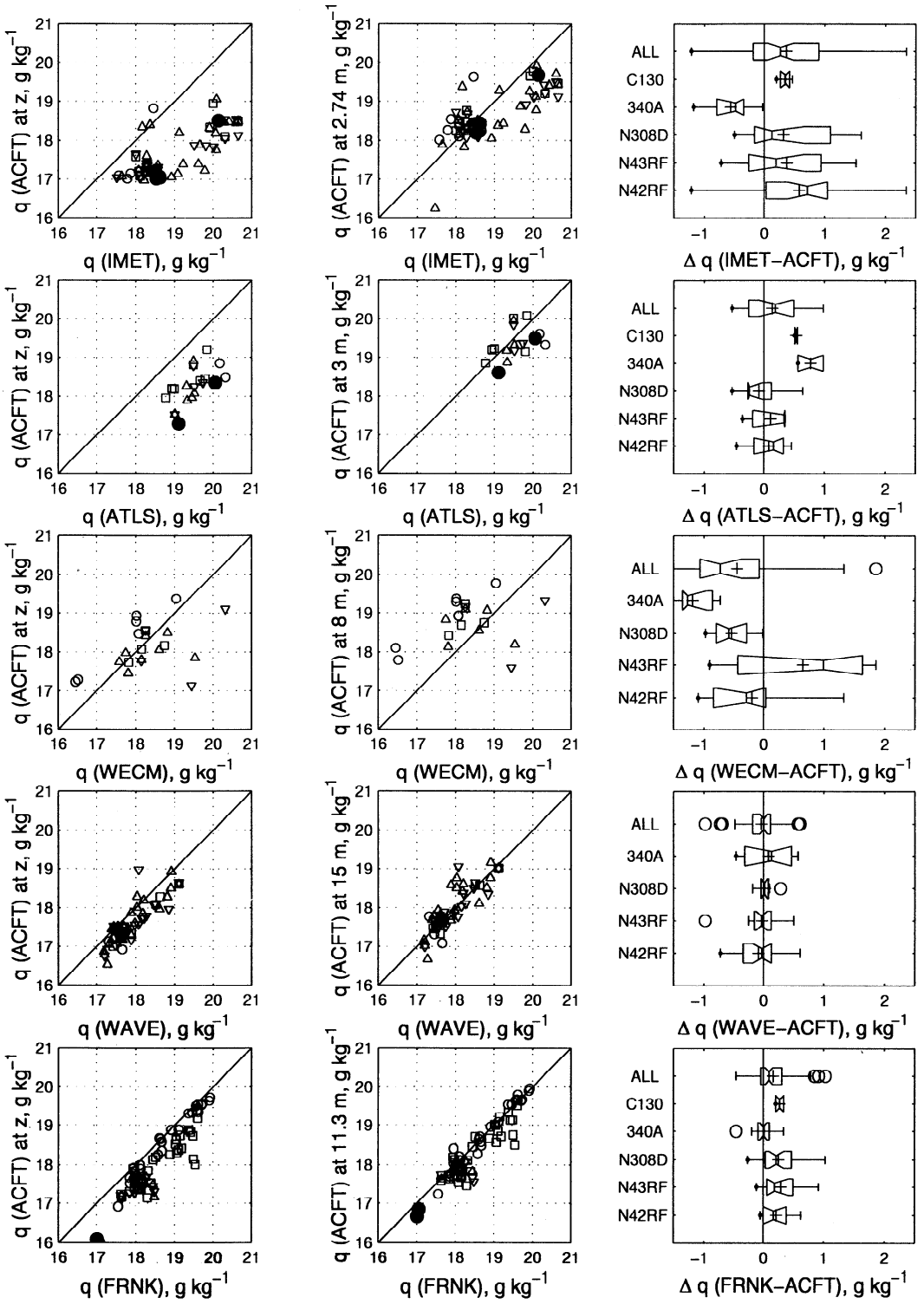

Figure 11. As in Figure 10 except that specific humidity q is compared here.

to the COARE bulk flux algorithm is sea surface "skin" temperature (SST). This measurement exhibited a high degree of variability among the five different aircraft. Corrections to aircraft SST (not discussed here) were applied to the aircraft radiometric surface-temperature measurements prior to any data height adjustments.

Unless otherwise noted, the ship and buoy data used in this study were measured by the instruments shown in Table 1. The data processing corrections made to the surface-platform data are summarized below. (The surface-platform corrections mentioned here are not part of the present study.)

The *Moana Wave T* and q measurements included a correction for daytime heating based on wind speed and solar radiation. In addition, the factory calibration for the Vaisala humidity sensor has been reduced 2% to

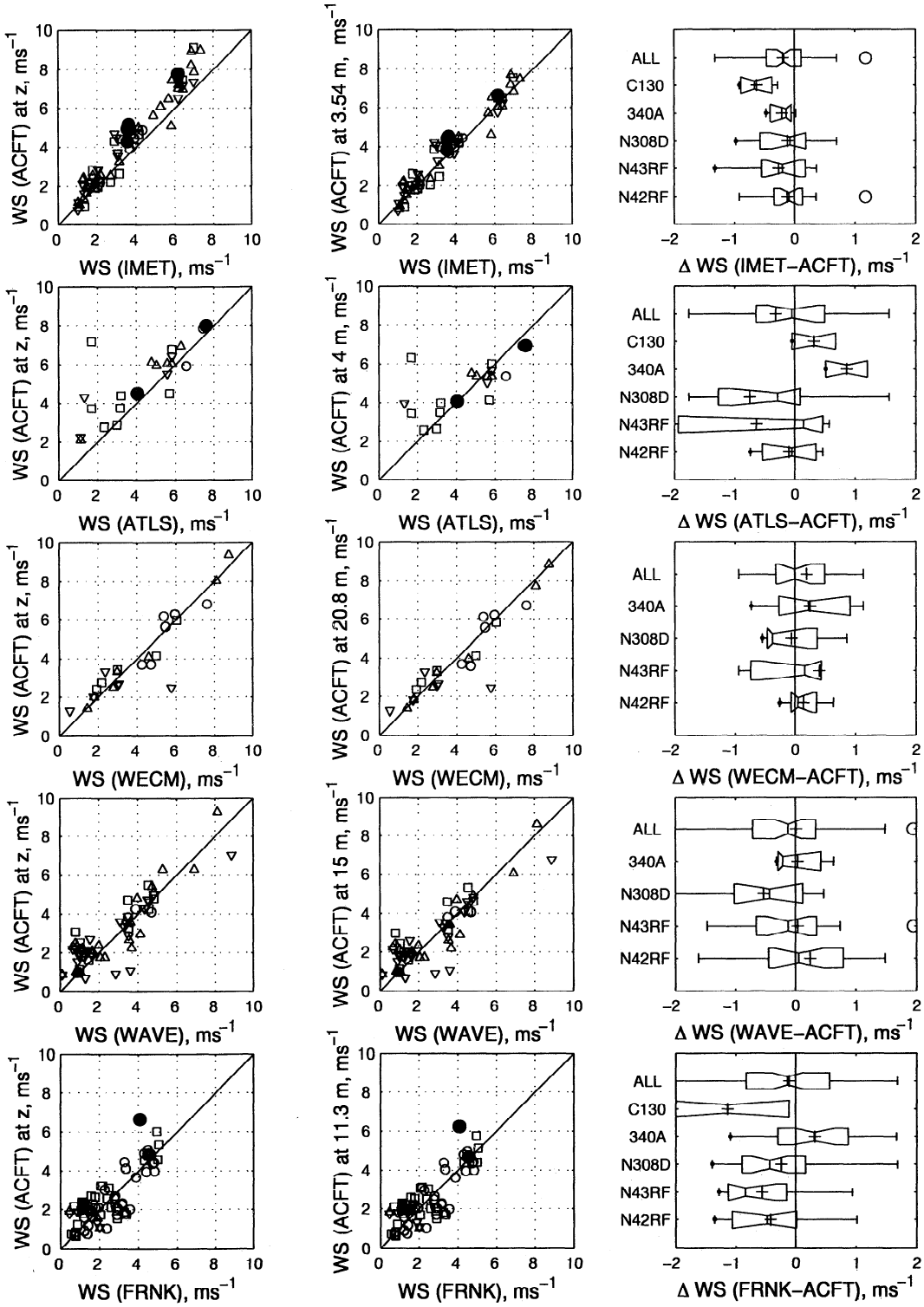

Figure 12. As in Figure 10 except that wind speed WS is compared here. Six IMET points are not shown due to cup anemometer "sticking."

force average agreement with another humidity sensor, an OPHIR IR-2000. The *Wecoma T* data were usually obtained from a shielded thermistor mounted on a bow mast 1 m toward the port side and 8 m above the water line. During the brief periods when this sensor was not working, data were taken from a second sensor located midship and portside. *Wecoma* had five different humidity sensors. The main instrument was a Vaisala humidity sensor probe mounted midship on the starboard side, 8 m above the water line. For a 3-day period in mid-November data from the portside Rotronics sensor were used. On the basis of previous wind speed comparisons between *Franklin* and *Moana Wave*, the *Franklin* data have been increased by 0.2 m s^{-1} and the *Moana*

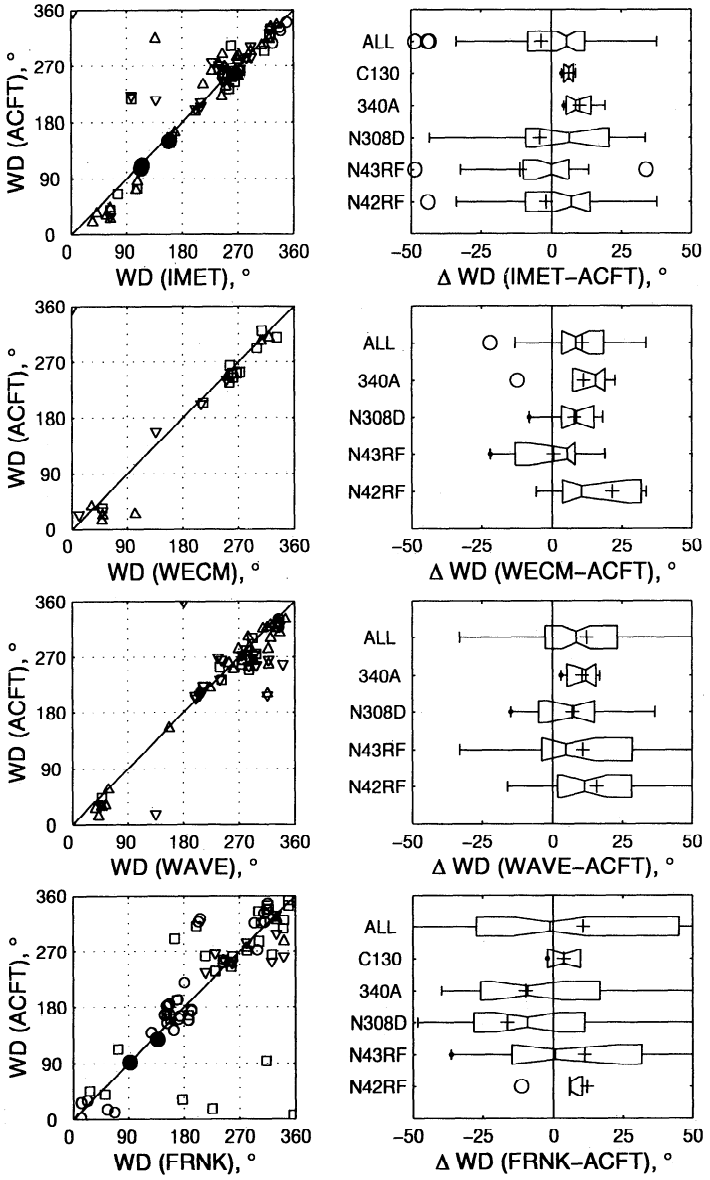

Figure 13. As in Figure 10 except that wind direction WD is compared here, and there is no height adjustment to aircraft data. (Data from ATLAS are not compared because of a wind vane malfunction.)

Wave data decreased by 0.2 m s^{-1}. On *Wecoma*, wind data from the port and starboard R.M. Young sensors were compared and brought into agreement. Then, data from the sensor that had the best exposure were used. Wind vector data from the ships are relative to the surface of the ocean.

The WHOI buoy moored at 156°E, 1.75°S (hereinafter called IMET) and the ATLAS buoy moored at 155.91°E, 1.99°S provided meteorological measurements below 4 m (the exact heights of the different sensors are given in Table 1). For this section, some unreasonably low IMET WS data (due to the anemometer sticking) have been eliminated from the comparisons. There were no IMET data for December 9-13, 1992. The ATLAS wind direction data were unusable for the IOP and its wind speed data were unreliable between October 26 and November 15, 1992.

A total of 267 proximate aircraft-surface platform comparisons were identified using the postflight technique detailed in Appendix B. The number of comparison points between the various platforms are given in Table 2.

Scatterplots and box plots of surface-platform data versus empirically corrected aircraft data (with the values given in Figure 5), at the aircraft measurement heights and after adjustment to the surface-platform heights, are shown for T (Figure 10), q (Figure 11), WS (Figure 12), WD (Figure 13), and BP (Figure 14).

With the exception of comparisons to IMET, the ambient temperature scatter was generally confined to within ±0.5°C. Above ~ 29°C, T from IMET was too high due to shortwave radiation heating. *Weller and Anderson* [1996] used an empirical formula to correct for this effect, and the IMET public-domain data file

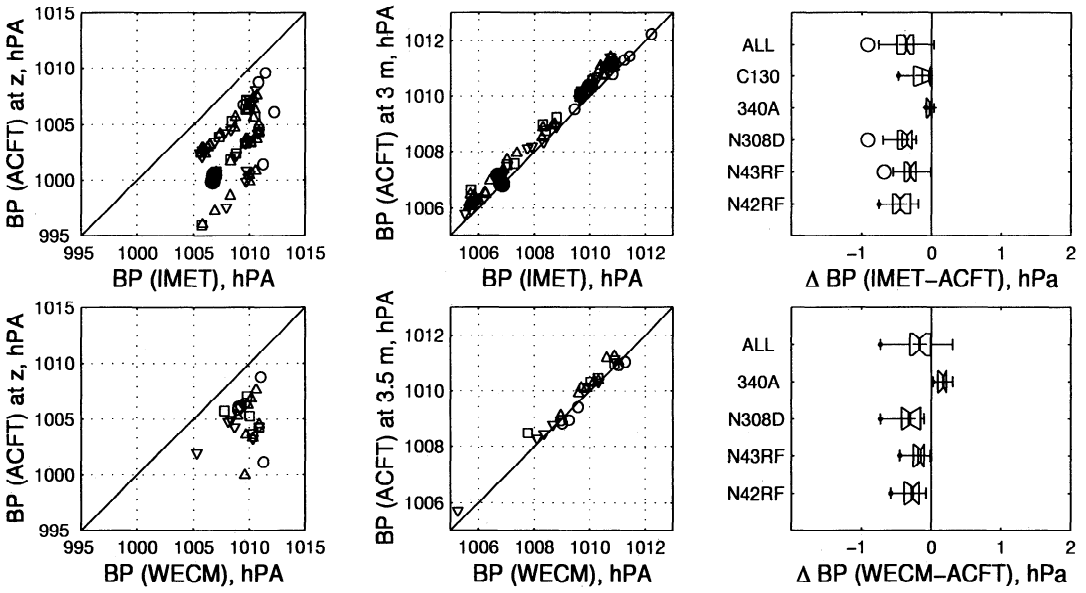

Figure 14. As in Figure 10 except that barometric pressure BP is compared here. There are no BP data from ATLAS, *Moana Wave*, and *Franklin*.

contains both uncorrected (or, raw) and corrected temperatures. For the relatively clear low-wind conditions of 921128, the formula appeared to overestimate the correction (this is discussed in more detail in Section 4 below). Since 921128 was specifically dedicated to comparison work among the ships, aircraft and the IMET buoy, many intercomparisons took place on this day (details are in Appendices A and B), and therefore we have chosen to use the uncorrected IMET temperature for the analysis in this section. The agreement was best when comparing with ATLAS. The three ships have temperature values on average $\sim 0.2°C$ less than those measured on the aircraft. The aircraft temperatures adjusted to the height of the temperature sensor on the surface platforms were found to be, as expected, greater than those measured at aircraft level. The height corrections were not as large for *Moana Wave* and *Franklin* because their temperature sensors located at 15 and 11.3 m, respectively, were much higher than the buoy sensors.

For specific humidity the agreement was best between the aircraft and *Moana Wave*, where most of the comparisons are within ~ 0.3 g kg^{-1}. There was also good agreement between the *Franklin* and 340A q during their numerous (26) intercomparisons. The four other aircraft had values of q about 0.3 g kg^{-1} less than those from *Franklin*. Since no BP measurements were made on ATLAS, q was calculated from the ATLAS relative humidity and the nearby IMET BP data. The ATLAS specific humidity agreed well with aircraft data except for 340A, and most of the comparisons were within $\sim \pm 0.3$ g kg^{-1}. The scatter was much greater when comparing with *Wecoma*, which had values of specific humidity ~ 0.3 to ~ 1.0 g kg^{-1} lower than those of the aircraft. Comparisons with IMET showed differences ranging from $\sim$ -1.0 to $\sim$ 2.0 g kg^{-1}. This may have been due to the radiative heating effect on the IMET ambient temperature that was used to derive q.

The aircraft wind speed data agreed best with IMET and *Wecoma* measurements where the scatter was within roughly ± 0.5 m s^{-1}. (Six overflights during periods when the IMET cup anemometer was "stuck" were excluded from this comparison.) The scatter doubled when comparing with *Franklin*, *Moana Wave*, and the ATLAS. It should be noted that *Moana Wave* operated as a drifter most of the time and therefore winds below 2 m s^{-1} were not reliable. Wind direction differences were about $\pm 25°$ when comparing with *Wecoma*, IMET, and *Moana Wave*, while comparisons with *Franklin* revealed a much larger scatter.

Aircraft barometric pressure measurements were compared to those from IMET and *Wecoma* only. (There was no pressure measurement on ATLAS and data from *Moana Wave* and *Franklin* were not available.) The pressures from aircraft elevation were adjusted to the height of the sensors on these two surface platforms using a simple adiabatic atmosphere model. Good agreement was found among C130, 340A, and IMET, whereas the three other aircraft were biased high by ~ 0.4 hPa. When compared with *Wecoma*, this bias was reduced to ~ 0.2 hPa, and the pressure measured on 340A was ~ 0.2 hPa smaller than that of *Wecoma*.

Figure 15 summarizes the comparisons presented in this section. The aircraft data were consolidated into one data set and compared to the combined data from the three ships and the combined data set from the two buoys. In general, the measurements are in reasonable agreement, and the scatter is within the accuracy of the instrumentation. To evaluate the effects of the empirical corrections on the comparisons, results with

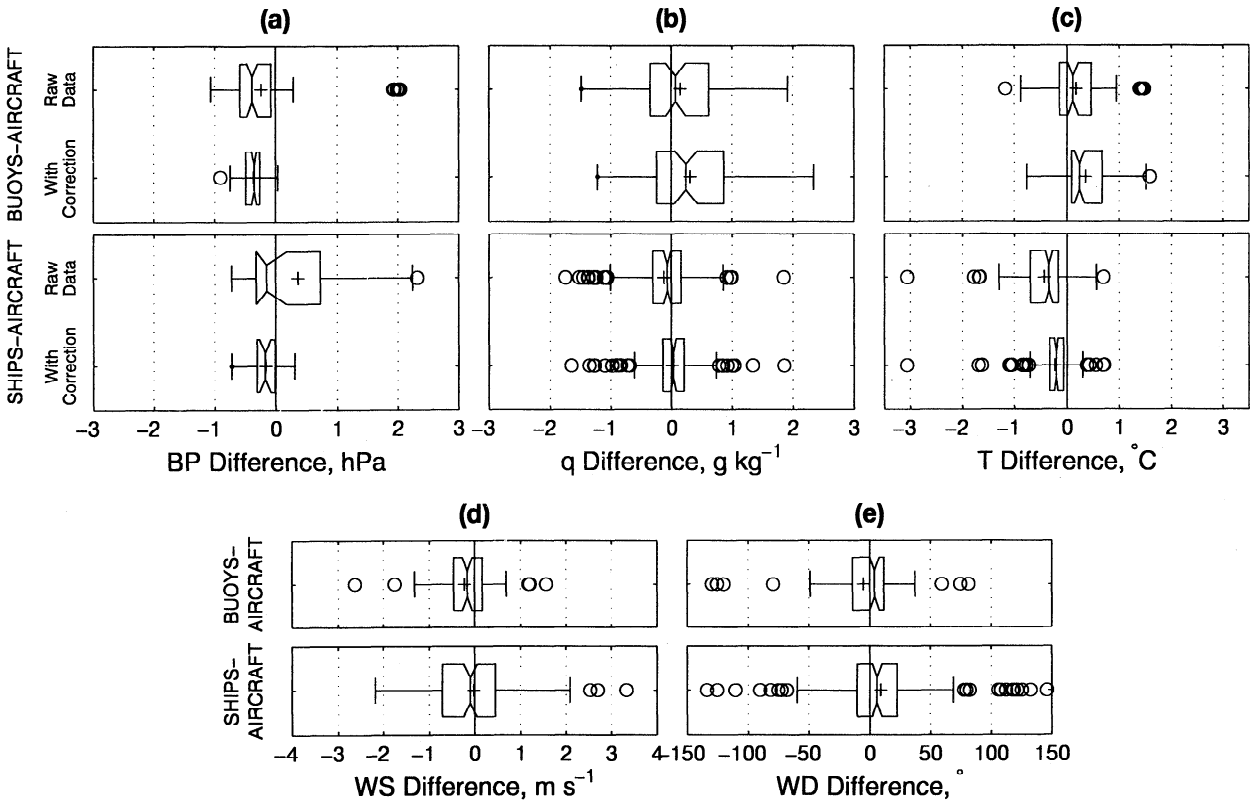

Figure 15. Box plots of mean differences between ship-aircraft and buoy-aircraft measurements of (a) barometric pressure BP, (b) specific humidity q, (c) ambient temperature T, (d) wind speed WS, and (e) wind direction WD. Individual platform data are combined based on platform type to form the aircraft, ship, and buoy data sets. For BP, q, and T, differences are shown with and without the aircraft empirical corrections.

and without corrections are presented. The corrections reduced the scatter in all comparisons except for q between buoys and aircraft. Wind comparisons are not affected by the corrections. Overall, the aircraft empirical corrections improved the aircraft-surface platform comparisons.

4. Single-Mission and Overall IOP Comparisons

The previous two sections have focused on specific aircraft wingtip-to-wingtip and aircraft-surface platform comparisons. It is also useful to compare statistics of these data for the whole IOP, regardless of platform spatial proximity, to further ascertain whether the proposed empirical corrections are consistent with the larger data set.

First, we consider time series of all low-level aircraft data on a given flight mission regardless of platform location, but primarily within the IFA. These data include both spatial (from aircraft) and temporal (from buoys and ships) variability over a period of 4–5 hours. Second, we examine the ensemble of all low-level aircraft data collected throughout the 4-month IOP as both time series and frequency distributions with and without the empirical corrections. This analysis is similar to the aircraft data comparisons in section 2.2.

4.1. Mission-by-Mission Comparisons

For a typical boundary layer mission, one to five aircraft flew to the IFA in daylight hours, while ships and buoys recorded surface measurements. Many missions were near the ships and buoys, but a few flights near the end of February were not. Since a typical aircraft leg covers 30-120 km in a relatively short time (5-20 min), these runs can be used to estimate spatial variability. Furthermore, if two (or more) aircraft were flying in the same vicinity, any differences between aircraft data that were greater than the spatial variability measured by a single aircraft can be attributed to systematic inaccuracies in the aircraft instrumentation. A single mission is used to illustrate these comparisons.

Before presenting these data, a short note regarding the adjustment of the surface-platform data to 10-m height is given. Of the surface platforms, the IMET and *Wecoma* data were adjusted to 10 m using the calculated "skin" temperature via the warm-layer and cool-skin algorithm in the COARE bulk formula [*Fairall et al.*, 1996a]. To calculate the other surface-platform

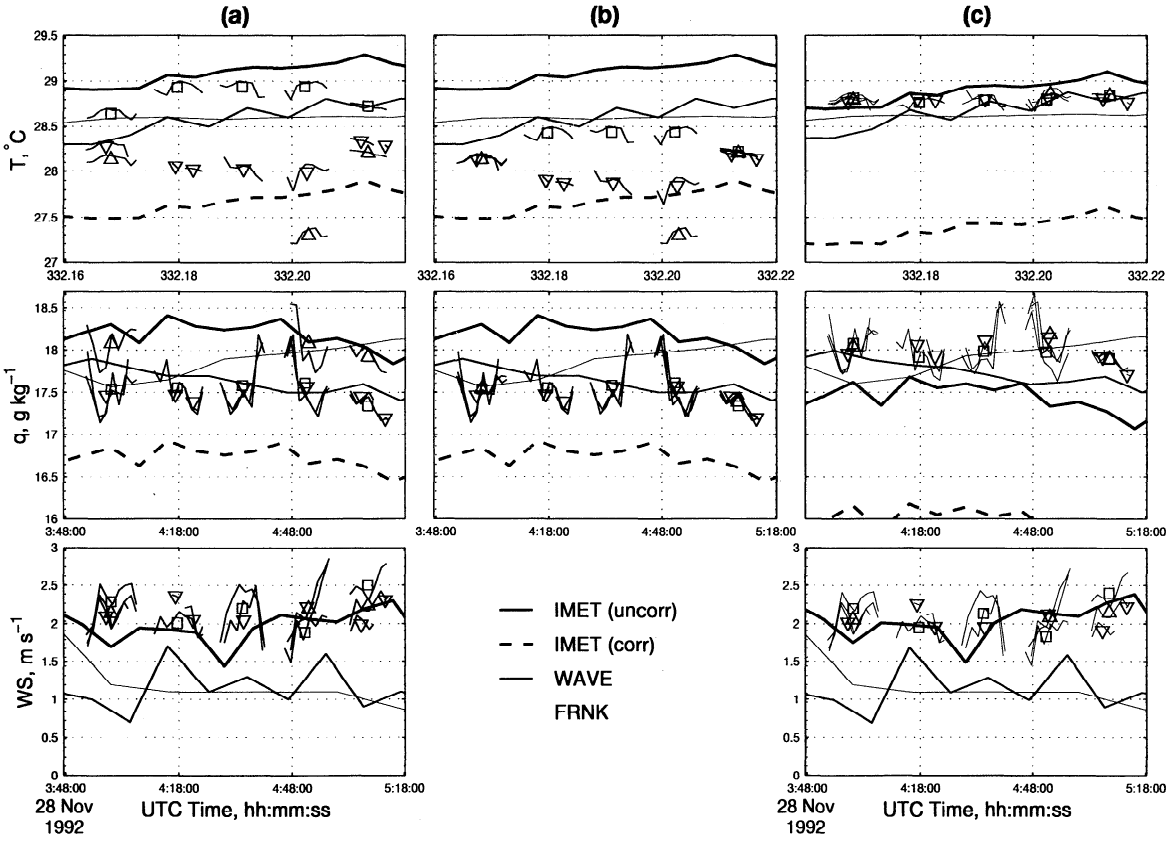

Figure 16. Surface platform ambient temperature T, specific humidity q, and wind speed WS time series along with aircraft 10-km (short lines) and leg-long mean values (symbols) from 921128 for (a) raw data, (b) empirically adjusted aircraft data, and (c) all data adjusted to 10 m. Aircraft symbols can be identified from Table 2. Dashed lines are IMET data corrected for radiant-heating errors. The Julian day (0 = 0:0:0 UTC, January 1, 1992) rounded to the nearest 0.01 is shown in the top row. The data of each row are identified on the far-left side.

10-m data, the sea temperature at the instrument location was used. For *Franklin* the SST data used were from the thermosalinograph at 2.4-m depth, not the infrared radiometer which did not operate continuously. The *Moana Wave* SST data used were obtained from a thermistor towed about 20 mm below the surface; that is, it captured the diurnal warming but not the cool skin.

The 921128 mission was part of a dedicated surface-layer comparison when ships and aircraft all converged near the IMET buoy. The weather was typical of suppressed conditions (COARE class 0) with low winds and relatively homogeneous and stationary meteorological conditions. Figure 16 shows 1.5 hours of aircraft, ship, and buoy time series for raw data (column a), raw data with empirical corrections (column b), and raw data with empirical corrections and adjustment to 10 m (column c). For the aircraft, 10-km-averaged data for each ~90-100 km track is shown along with the leg-long mean values (symbols). Both raw and corrected IMET air temperatures are shown, and the effect of using these temperatures to convert from relative to specific humidity. Application of the aircraft empirical corrections (Figure 16b) brings all aircraft ambient temperatures at measurement height below those of the near-surface platform, as we would expect for adiabatic or unstable conditions. The adjustment of all platform data to 10 m (Figure 16c) improves agreement and indicates why we chose to use the uncorrected-for-solar-heating IMET ambient temperature for section 3 comparisons (where 921128 was an important mission).

A longer time series of the 921128 mission is shown in Figure 17, which reveals the solar heating of the IMET temperature sensor peaking at around 630 UTC (1730 LT). The correction applied by *Weller and Anderson* [1996] brings this peak temperature into agreement with the ships but results in overcorrection earlier on this day of very light winds and clear skies; however, if data from many missions are considered (as will be done in section 4.2), the IMET solar heating correction shows better agreement with the aircraft and other surface platform data. The late-afternoon maximum of solar heating errors in unaspirated temperature sensors has been explored by *Anderson and Baumgartner* [1998].

The bottom panels of Figure 17 show IMET wind

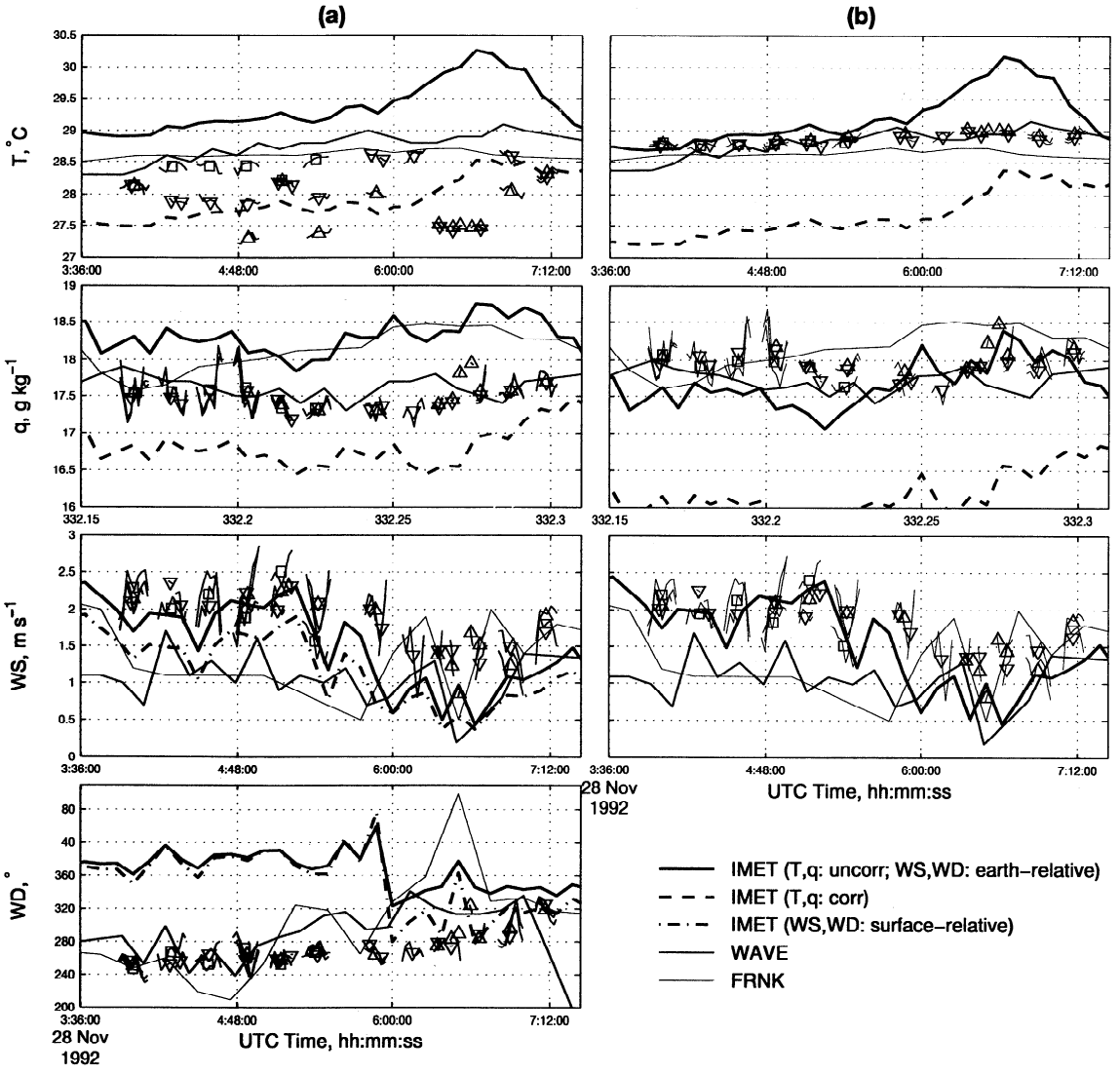

Figure 17. Surface platform ambient temperature T, specific humidity q, and wind speed WS and direction WD time series, along with 10-km (short lines) and leg-long mean values (symbols) from 921128 for (a) empirically adjusted aircraft data and (b) all data adjusted to 10 m. Aircraft symbols can be identified from Table 2. For IMET, solar-heating corrected and uncorrected (dashed) T and q data are shown; IMET WS and WD are shown relative to the Earth (solid) and the surface (dotted-dashed). The ships wind data are relative to the ocean surface. The Julian day (0 = 0:0:0 UTC, January 1, 1992) is shown in row 3.

speeds substantially higher than those measured on the ships *Franklin* and *Moana Wave*. This is partly because the IMET winds shown are Earth-relative, whereas the ship winds are relative to the surface of the water, as required for the calculation of bulk fluxes. *Franklin* obtains relative winds by using the log/gyro of the ship, and the *Moana Wave* by applying the current measured at 5 m depth on IMET. Similar correction to IMET winds results in a substantial reduction to WS on this day, as shown in Figure 17. Given the instrumental difficulties in measuring such very light winds, and surface current corrections of the same magnitude, better agreement than shown here can hardly be expected.

The complete 4-month IOP time series of T, q, WS (all adjusted to 10 m), BP (adjusted to the surface), and WD (no adjustment) are plotted in Figures 18 and 19. Since no aircraft-surface platform comparisons occurred at night, the buoy and ship daytime data variations were captured by averaging over the daylight hours only. The ~ 12-hour daylight time period used is shown in Figure 7d and was determined from the IMET solar radiation data. Also identified in Figures 18 and 19 are significant COARE meteorological events, such as the westerly wind burst, squalls, and low winds, as identified by *Weller and Anderson* [1996].

Differences between the buoy and the ship data were due to a combination of measurement errors and real variability present in the daytime-mean data. *Weller and Anderson* [1996] reported excellent agreement of mean observables among the IMET, *Moana Wave*, and

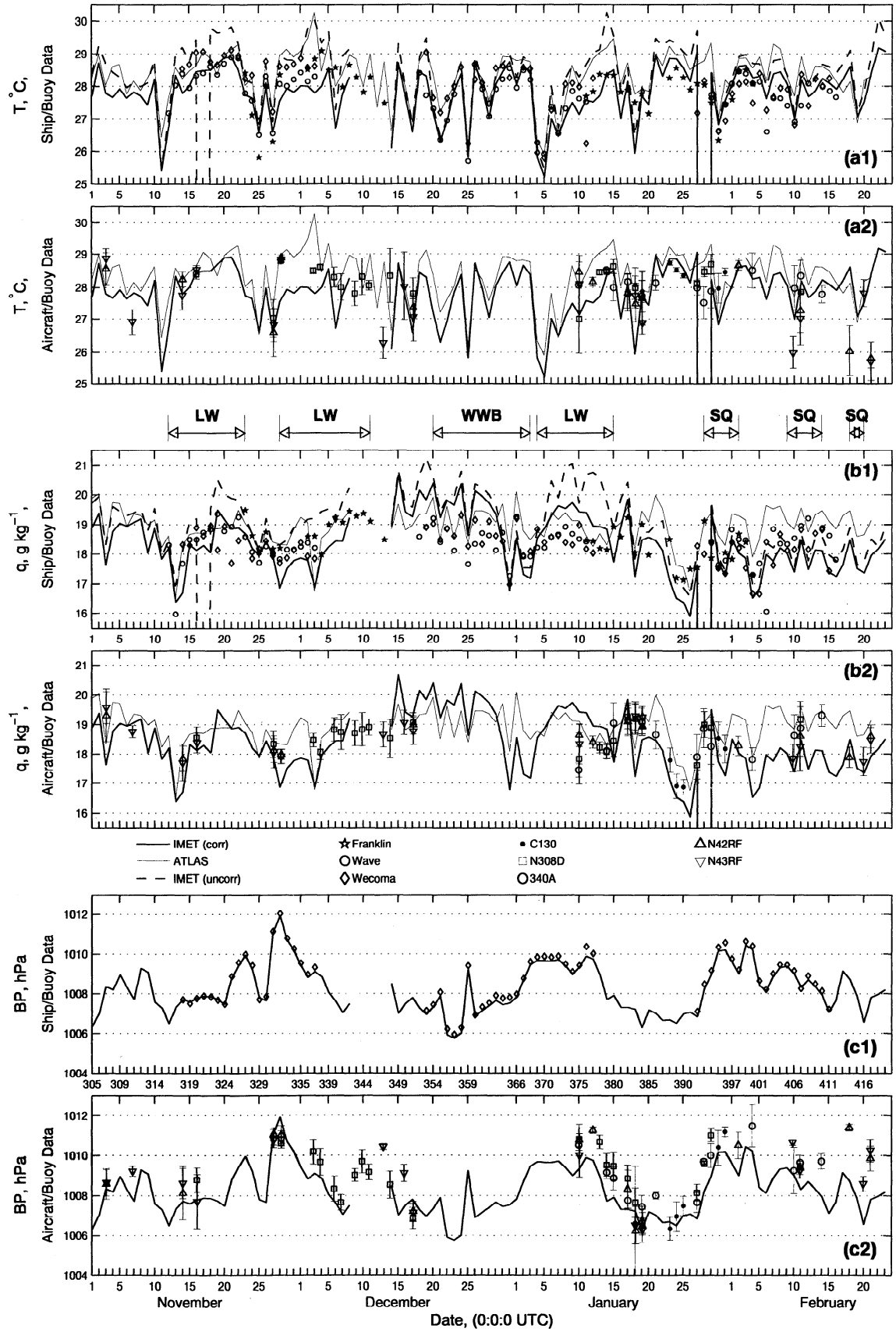

Figure 18. IOP time series of (a1-a2) ambient temperature T, (b1-b2) specific humidity q, and (c1-c2) barometric pressure BP. Aircraft T and q data are adjusted to 10 m.; BP is adjusted to the surface. Symbols are low-level 10-km means with vertical bars representing the standard deviation of all 10-km mean values for the mission. Buoy and ship data are daylighthour mean values (T and q adjusted to 10 m). Identified meteorological events are low-wind events (LW), westerly wind bursts (WWB), and squalls (SQ) as from *Weller and Anderson* [1996]. The Julian day (0 = 0:0:0 UTC, January 1, 1992) is shown in Figure 18c1. IMET data between UTC December 9-13, are excluded due to sensors being changed.

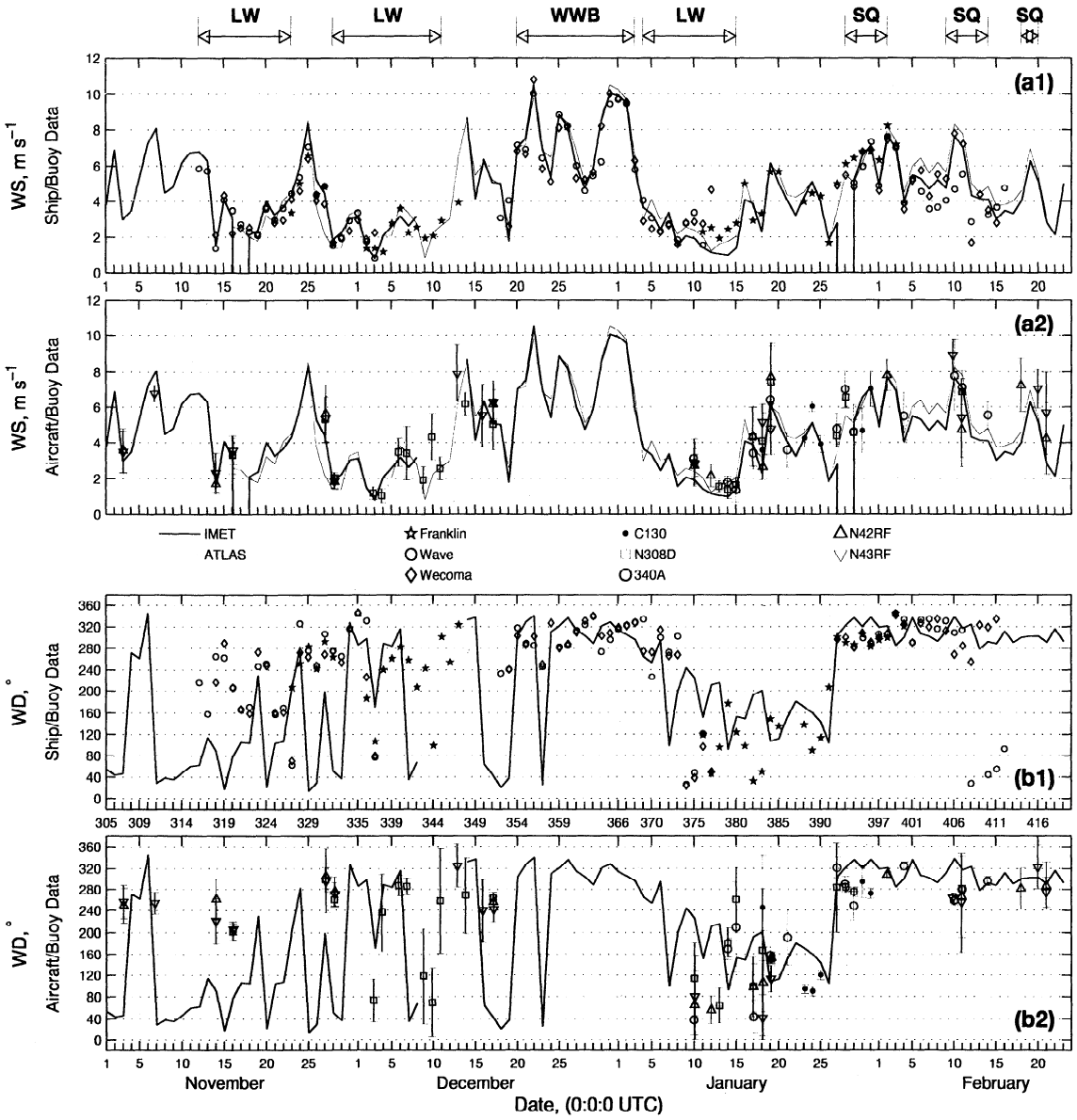

Figure 19. IOP time series of (a1-a2) wind speed WS and (b1-b2) wind direction WD. See Figure 18 for details (for WD the daylight-median value is used instead of the mean). ATLAS WS data (from UTC, October 26, 2100 to November 15, 2300) and WD data (entire IOP) are not shown due to sensor malfunction.

Wecoma over the duration of the three ship legs near IMET (the three ship legs were 19, 23, and 7 days long, respectively). In general, we found the comparisons between ships and buoys reasonable; a possible exception is the IMET q data between December 14, 1992 and January 15, 1993, when the IMET data appeared to be greater than the ships (Figure 18b1). There were not many aircraft missions during this period, but the flights in mid-December and early January also indicated IMET data were high. This time period included both a westerly wind burst and a low-wind event. The ATLAS q also indicates that IMET q was high during this period, though not so large a difference as between IMET and the ship/aircraft q data. There were also large differences between ATLAS and IMET q in February, but for this period, the IMET data were in agreement with the ship and aircraft data, and the ATLAS data were relatively higher.

4.2. IOP Ensemble Comparisons

An ensemble-type comparison of the aircraft, ship, and buoy data was achieved by combining all low-level data collected by each of the five aircraft (see section 2.2, Figure 8) to create one set (the "aircraft" set) and then conditionally selecting the ship and buoy data corresponding to the low-level aircraft flight periods. In other words, surface data were selected based on time periods when the aircraft were flying low-level

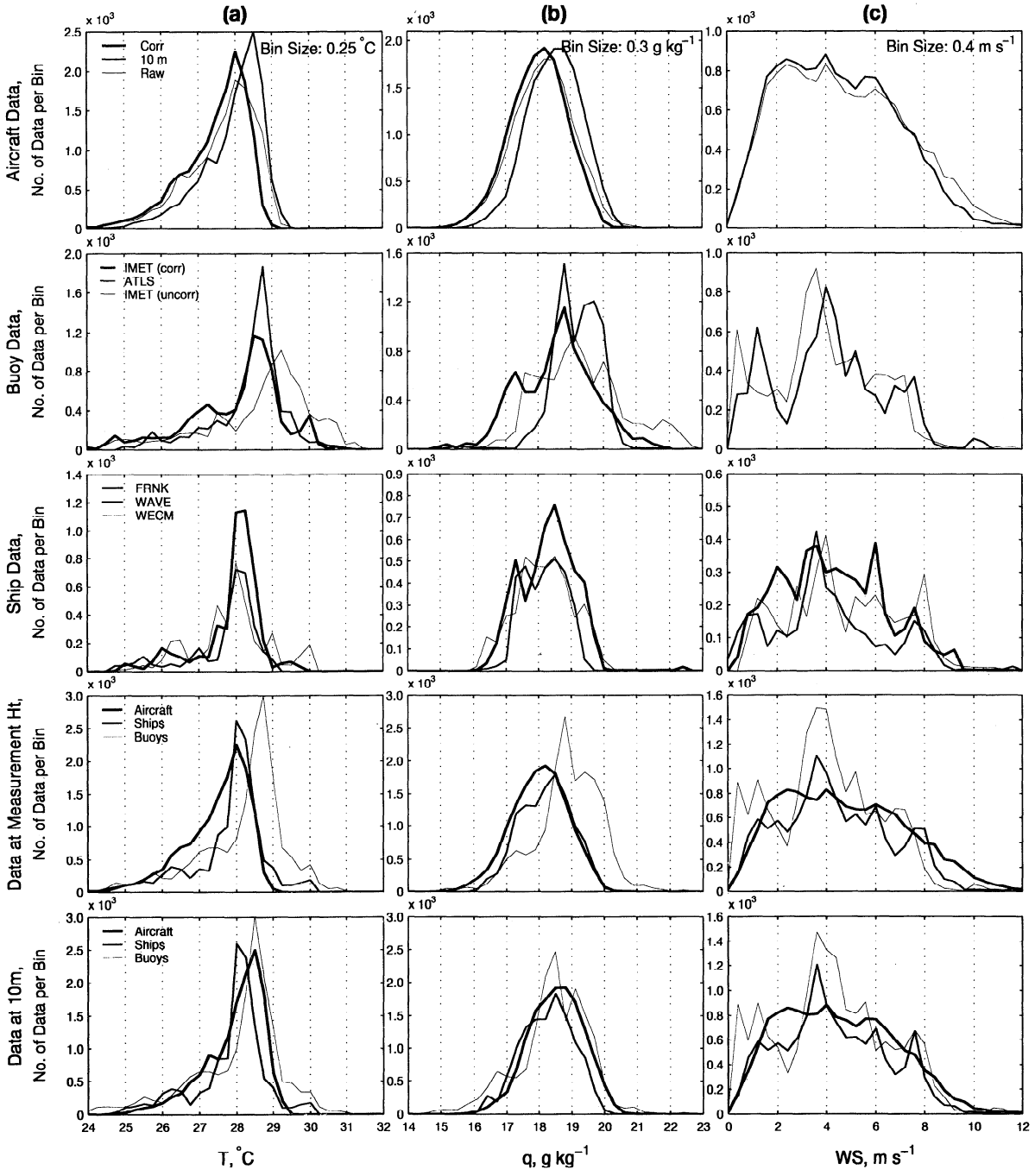

Figure 20. Frequency distributions of (a) ambient temperature T, (b) specific humidity q, and (c) wind speed WS for all aircraft low-level-run data. Buoy and ship data are from corresponding time periods between the start and the end of the aircraft low-level runs for all missions. See text for more information. The data of each row are identified on the far-left side.

runs (ship data were also restricted to be within the latitudes and longitudes shown in Figure 7). Since the surface platform sampling rates differed, all surface platform data were linearly interpolated to a rate of 0.0167 Hz (1 sample/min). To create the aircraft data set of the same approximate size as the combined-ships and combined-buoy data sets, every 25th point from the 1-Hz aircraft data set was selected. (The effect of using every 25th point or all 1-Hz data on the aircraft frequency distribution shape was minimal.) After the data-extraction technique was performed on all missions, it resulted in 14,190, 12,020, and 16,000 samples for the aircraft-, ship-, and buoy-combined data sets, respectively. Since the samples are obtained conditionally, based on the low-level aircraft run times, they do not reflect the entire spectrum of COARE conditions but do mostly represent the moderate-to-low-wind suppressed daylight conditions.

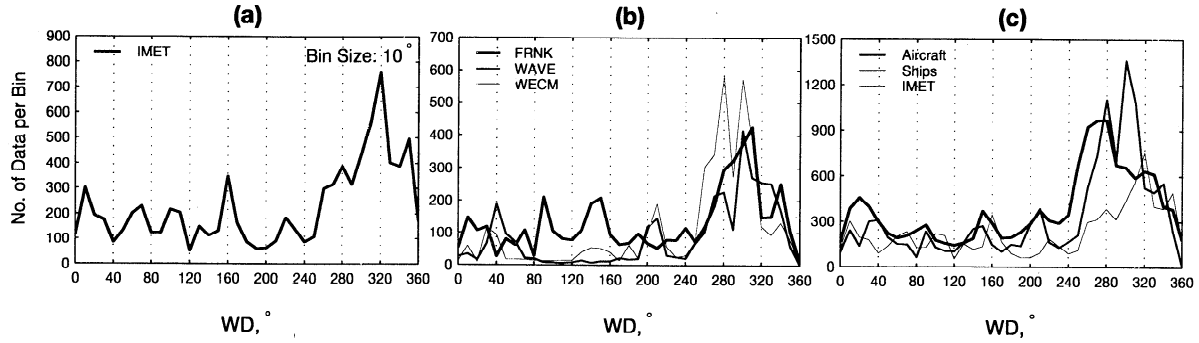

Figure 21. Same as Figure 20 except for wind direction WD (meteorological convention). The ATLAS WD data are not included due to a malfunction in the ATLAS wind vane.

Frequency distributions of the aircraft, buoy, and ship samples are shown in Figure 20 for temperature, humidity, and wind speed. Wind direction frequency distributions are in Figure 21. The solar-heating-corrected IMET temperature data agrees better with T from the ATLAS buoy, but the increased number of samples for $T < 28°C$ may indicate some overcorrection occurred (e.g., Figure 17). Wind speed agrees well, but both buoys, especially IMET, show many samples of extremely low WS data (0-0.8 m s^{-1}) which were not measured by either the ships or the aircraft. Some of these low WS data may be the result of the IMET cup anemometer "sticking." These data were excluded from the comparisons in section 3 but are included here for completeness. Any cup anemometer "sticking" was infrequent and did not appear to affect the daylight-mean IMET WS data (Figure 19). The IMET WS frequency distribution appears much different than the WS histogram of *Weller and Anderson* [1996, Figure 5] due to the conditional sampling we have used which emphasizes lower wind speed conditions.

Figure 20 also shows the frequency distributions of the combined aircraft, ship, and buoy data at their respective measurement heights (row 4) and adjusted to 10-m height (row 5). The T, q, WS (at 10 m), and WD (Figure 21) distributions show good agreement among the platforms. These curves reveal that the probability distributions of temperature, specific humidity, and wind speed are different. Ambient temperature at 10 m is skewed, with a rather sharp cutoff for temperatures above 29°C. However, that for specific humidity is not skewed and has a more Gaussian shape. The wind speed distribution is broad. The WD frequency distributions are generally consistent, showing that when the aircraft were flying at low levels, the wind was most frequently coming from the west-northwest direction (260°-330°).

5. Discussion and Conclusions

Comparison of the low-level COARE aircraft data from the comparison flights revealed the need for empirical corrections to bring the temperature, humidity, pressure, and radar altitude data into agreement. Some parameters required flight-date-dependent corrections, perhaps due to the long period (4 months) that the aircraft were in the field without sensor recalibrations. After empirical corrections were made, the differences among the aircraft were smaller than the basic sensor accuracies. The horizontal wind speeds and directions did not require additional corrections beyond those performed by the respective data processing facilities.

The corrected aircraft data were compared to the COARE ship and buoy data for overpasses within a radius of 15 km of the ship or buoy and heights below 100 m; the ship or buoy data were interpolated in time to match the aircraft overflight time. The height adjustment of the aircraft data down to the individual sensor heights on the surface platforms used the bulk-formula scheme of *Fairall et al.* [1996b]. Some comparisons were made between aircraft profile and level track data to the platform data and the bulk-formula extrapolation to the platform heights. The individual profile extrapolation results showed scatter, perhaps due to the spatial and temporal separation between the profiles and platform data. However, overall, the use of the bulk-formula scheme brought the extrapolated aircraft and platform data into good agreement. This may be due to the bulk-formula extrapolation having consistent properties, for example, wind speed always decreases down toward the surface, rather than having all of the underlying assumptions correct, such as a constant flux layer. Even though the extrapolation of COARE data appears to work well for heights up to 175 m, we chose to use a more conservative upper limit of 100 m.

On the basis of the good agreement between the extrapolated low-level aircraft and the surface platform data, all data available from the low-level aircraft flight time periods were adjusted to the traditional reference height of 10 m, irrespective of platform locations. Comparison of the resulting large set of aircraft and surface platform data also showed good agreement between the various platforms. Therefore it appears that an accurate surface-layer aircraft, ship, and buoy data set can be formed for COARE with the corrections presented in this study.

The means and standard deviations of the differ-

Table 4. Mean Measurement Accuracy Summary of Differences Between Aircraft Wingtip-to-Wingtip, Ships-Aircraft, and Buoys-Aircraft Comparison Data

	Measurement Differences					
	Figures 3, 4, & 6	Figure 15		Ensemble Values, Figure 20, Row 5		
Parameter (units)	Wingtip-to-Wingtip[a]	Ships-Aircraft	Buoys-Aircraft	Aircraft	Ships	Buoys
T, (°C)	0.06 ±0.08 [0.45 ±0.13]	-0.2 ±0.4 [-0.4 ±0.5]	0.4 ±0.4 [0.2 ±0.5]	27.9 ±0.8	27.9 ±1.0	28.1 ±1.2
q, (g kg^{-1})	0.01 ±0.07 [0.41 ±0.11]	0.0 ±0.5 [-0.1 ±0.5]	0.3 ±0.7 [0.2 ±0.7]	18.5 ±0.8	18.2 ±0.8	18.4 ±1.1
BP, (hPa)	0.1 ±0.2 [0.8 ±0.2]	-0.2 ±0.2[c] [0.4 ±1.1]	-0.4 ±0.2[b] [-0.2 ±0.6]	1009.1 ±1.6	1009.7 ±1.5[c]	1008.8 ±1.7[b]
WS, (m s^{-1})	0.1 ±0.3	0.0 ±1.0	-0.2 ±0.8	4.5 ±2.3	4.3 ±2.2	4.3 ±2.3
WD[d], (°)	2.0 ±8.2	6 ±68	4 ±37	254 ±104	276 ±99	266 ±113[b]

Ensemble measurement statistics (mean ± standard deviation) are also given. See figure number(s) given in the second row for more information about data used to determine statistics. For parameters with two values, the upper values are with both physical and empirical corrections to aircraft data, and the lower values (enclosed in brackets) are using aircraft data with physical corrections, but no empirical corrections.

[a]Wingtip-to-wingtip aircraft accuracy is estimated by using statistics from all five wingtip-to-wingtip combinations. The first value is the mean of the absolute value of the mean differences between each pair (the absolute value is used, so the result is independent of which aircraft is considered "reference" in taking the difference). The second value (shown after the "±") is the mean of the standard deviation of the mean difference for each combination.

[b]For buoys, IMET data only.

[c]For ships, *Wecoma* data only.

[d]For wind direction ensemble values the median is used instead of the mean.

ences among the platforms are shown in Table 4 for the aircraft wingtip-to-wingtip, ship-aircraft, and buoy-aircraft comparisons. The effect of the empirical corrections on the comparison statistics is evident in this table. After applying the empirical corrections, most mean differences are small and meet the mean data accuracy criterion necessary to achieve the COARE goal of measured total averaged surface latent and sensible heat fluxes to within ±6-7 W m^{-2}. Also in Table 4, the mean values from the ensemble comparisons are included. It should be noted that even though there may be some bias in the ensemble statistics due to spatial differences in the data sampling, the overall values are in close agreement.

While the above results are encouraging for future analyses of the COARE aircraft data set, the determination of empirical corrections is at present a necessary but primitive way to meet the desired accuracies. In principle, empirical corrections should not be required for aircraft measurements since the methodology is based on well-known exact fundamentals (e.g., the compressible flow equations). However, there are many error sources, such as the placement of sensors on the aircraft (flow distortion), interrelatedness of measurements (e.g., static and dynamic pressures required for ambient temperature), secondary effects (e.g., calibration changes), etc., that combine to affect the overall data accuracy. While the use of empirical corrections accounts for most of these errors, a more thorough solution is to identify the error sources and correct for them. Some additional procedures that might improve data integrity would be to conduct preexperiment comparisons in conditions approximately similar to those expected in the field campaign and to perform instrument recalibrations during long field deployments. More research on the fundamentals and details of aircraft measurements should eliminate, or at least minimize, the need for empirical corrections.

Appendix A: Aircraft Data Details

A1. Data Sources

The COARE boundary layer aircraft data used in this study were processed by several different data processing centers. For the WP-3Ds and N308D the flight-level data were processed by more than one group. In addition, many of these data have been processed several times and therefore have several different release dates or versions. The purpose of this appendix is to serve as a guide for investigators who are interested in using aircraft data that are consistent with the results shown in this paper. Unless specified, the corrections discussed in this paper are not included in data obtained from the data processing center. The National Climatic Data Center (NCDC) maintains much of the TOGA COARE data, which were also placed in a "deep

Table A1. Acquisition Details of TOGA COARE Aircraft Data

Aircraft	Data Type/Format	Data Processor	Release Date
NOAA WP-3D	MATLAB/ASCII (1 Hz)	UC Irvine, USA	January 15, 1998[a]
NCAR N308D	binary "Genpro" (20 Hz)	NCAR/ATD, USA	April 27, 1994[b]
	ASCII (1 Hz)	New Mexico Tech, USA	September 30, 1993[c]
MRF C130	ASCII level runs (1 Hz)	MRF, UK	July 1, 1995[d]
FIAMS 340A	binary "stream" (~ 20 Hz)	FIAMS, Australia	March 1, 1995[e]

[a]http://wave.eng.uci.edu/; Carl Friehe (cfriehe@uci.edu).
[b]NCAR mass store system; Richard Chinman (chinman@ucar.edu).
[c]ftp://mrd3.mmm.ucar.edu/pub/TOGA-COARE/electra/;
Dave Raymond (raymond@kestrel.nmt.edu).
[d]http://wwwarc.essc.psu.edu (note: no longer available here);
Phil Hignett (phignett@meto.govt.uk).
[e]Obtained on a Digital Audio Tape (DAT);
Jörg Hacker (j.hacker@es.flinders.edu.au).

archive" at NCAR. Aircraft data used in this study and how they were obtained are shown in Table A1. Investigators wishing to obtain TOGA COARE data should contact NCDC (NCDC, Asheville NC 28801-5001, http://www.ncdc.noaa.gov/) to find the latest information.

For our study the 340A and N308D 1-Hz data sets were "created" by down-sampling the full-resolution 20-Hz data. For the 340A data, a 1-s boxcar averaging technique was used, while for N308D, every 20th point was picked off. Different down-sampling techniques were used since the 340A 20-Hz data were prior-adjusted to be equidistant in space, not in time (see *Williams and Hacker* [1993] for details). The MRF-determined C130 empirical corrections (-0.75°C for T_d, +0.55°C for T) were removed from the 1-Hz data prior to the comparisons in this study (see the documentation with C130 data, obtained from the location shown in Table A1).

As mentioned in the introduction, the WP-3D data used in this study were processed by UCI. Another WP-3D data set, processed by the National Severe Storms Laboratory (NSSL), is also available. Since the NSSL data have temperature and dew-point corrections based on balloon flybys, the WP-3D corrections determined in our study are not directly applicable to the NSSL-processed data. Information and corrections for the NSSL data are described by *LeMone et al.* [1998]. The corrections to the NSSL-processed data were determined by taking into consideration the findings of the present study and should lead to fairly consistent mean values between the UCI-corrected and the NSSL-corrected data sets. To aid researchers in determining if they are using data consistent with the findings of our study, Table A2 includes mean values of empirically corrected temperature and humidity from the comparison periods. These values can be used to confirm data compatibility with the findings of our study.

A2. Wingtip-to-Wingtip Comparison Details

A complete listing of the aircraft wingtip-to-wingtip comparison legs used in this study is in Table A2. This table includes exact UTC times, identifies the lead aircraft (based on the magnitude of the deviations in the track angle), and shows the mean elevation, track angle, temperature, and dew point (for 340A specific humidity is shown) of each aircraft during the aircraft-aircraft comparison legs. An example of the relative positions of the aircraft during a three-aircraft comparison leg is shown in Figures A1a and A1b. The aircraft positions have been translated into the coordinate system of the leading aircraft (in this case, N43RF), and the positions of N42RF and N308D are shown relative to the leader. Aircraft positions are from INS/GPS blended data; this improves the relative accuracy of the raw INS position data by about a factor of 50. In Figure A1b, the N308D data are more scattered due to the lower resolution of the position data supplied by NCAR (~ 111 m; the WP-3D data have a resolution of around 10 m). The 1-m resolution of the WP-3D APN-232 radar altimeter is revealed in Figure A1a.

The aircraft positions relative to the lead aircraft for all the comparison legs involving N42RF and N43RF are shown as frequency distributions in Figures A1c

Table A2. TOGA COARE Aircraft-to-Aircraft Comparison Time Periods and Mean Values for Empirically Corrected Radar Altitude H_r, Track Angle trk, Empirically Corrected Ambient Temperature T, Empirically Corrected Dew Point T_d, and Empirically Corrected Specific Humidity q (340A Only)

Flight	Lead	UTC	Time	C130, 340A, or N43RF				N308D				N42RF			
ID[a]	A/C	(start)	(s)	H_r	trk	T	(T_d or q)	H_r	trk	T	T_d	H_r	trk	T	T_d
921102															
HI.1a	N43RF	001945	500	65.9	39.9	28.00	24.38	-	-	-	-	66.7	40.0	27.96	24.40
HI.1b	N43RF	003420	400	64.2	33.0	28.02	24.47	-	-	-	-	64.6	33.0	27.99	24.47
HI.1c	N43RF	004120	300	62.7	34.5	28.17	24.54	-	-	-	-	62.2	34.5	28.16	24.55
921113															
HI.01	N43RF	224600	900	156.6	26.2	26.91	23.29	-	-	-	-	155.9	26.2	26.93	23.31
HI.02	N43RF	230500	1300	66.4	340.0	27.46	22.89	-	-	-	-	67.1	340.0	27.47	22.88
921115															
EI.01	N308D	000430	1300	61.7	269.7	27.79	23.07	62.6	269.6	27.79	23.14	-	-	-	-
921126															
EHI.01	N43RF	020100	500	65.0	269.8	26.31	22.87	64.0	269.7	26.36	22.85	64.7	269.8	26.33	22.85
921128															
EHI.01	N42RF	035400	700	62.7	178.7	28.13	22.81	65.8	174.1	28.14	22.83	65.4	176.1	28.14	22.85
EHI.02	N42RF	050300	600	62.7	60.1	28.18	22.75	64.7	60.0	28.22	22.70	64.7	60.1	28.20	22.75
HI.4a	N42RF	062040	100	156.1	79.1	27.45	22.58	-	-	-	-	156.2	79.4	27.49	22.61
HI.4b	N42RF	062620	100	157.3	260.0	27.43	22.59	-	-	-	-	156.5	260.1	27.48	22.62
HI.4c	N42RF	062930	100	157.5	350.0	27.45	23.02	-	-	-	-	157.4	349.8	27.49	23.06
HI.4d	N42RF	063430	100	155.7	170.1	27.44	23.08	-	-	-	-	157.3	170.0	27.47	23.10
HI.05	N42RF	063700	300	155.6	149.8	27.45	22.67	-	-	-	-	156.7	149.7	27.48	22.71
HI.06	N43RF	070500	600	67.4	150.9	28.27	23.05	-	-	-	-	67.0	150.9	28.32	23.05
921216															
HI.01	N43RF	011330	500	177.3	304.2	25.55	23.51	-	-	-	-	178.1	304.2	25.53	23.52
EHI.02	N43RF	015800	600	63.3	19.4	26.57	23.72	63.1	19.4	26.60	23.72	65.0	19.4	26.55	23.73
930109															
EHI.01	N43RF	225100	300	204.7	340.0	26.48	22.81	207.4	340.1	26.49	22.87	207.2	339.9	26.47	22.85
EHI.02	N43RF	230000	1300	62.8	270.2	27.93	23.55	61.7	270.3	27.92	23.56	61.4	270.2	27.96	23.53
HI.3a	N42RF	025300	100	162.5	188.4	27.19	23.15	-	-	-	-	159.7	188.7	27.23	23.10
HI.3b	N42RF	025700	100	153.1	9.3	27.31	22.98	-	-	-	-	158.4	9.6	27.28	22.94
HI.3c	N42RF	030030	100	153.9	277.3	27.26	23.01	-	-	-	-	155.6	277.4	27.28	22.98
HI.3d	N42RF	030445	95	159.6	99.6	27.23	22.84	-	-	-	-	157.9	99.6	27.28	22.81
930113															
EF.01	N308D	230920	40	56.1	276.9	27.98	17.62	64.1	277.6	27.91	22.97	-	-	-	-
EF.02	N308D	231830	40	59.7	94.9	27.85	18.11	59.7	89.8	27.97	23.25	-	-	-	-
930114															
EF.01	N308D	230700	30	56.8	183.7	28.11	17.59	57.3	181.3	28.26	23.03	-	-	-	-
EF.02	N308D	232520	30	57.6	1.9	28.18	17.51	61.7	116.6	28.21	22.89	-	-	-	-
930116															
EH.02	N42RF	233830	1200	-	-	-	-	65.5	90.1	27.02	23.78	64.7	90.1	26.99	23.76
EH.03	N42RF	000700	700	-	-	-	-	216.8	270.3	26.30	22.76	212.9	270.4	26.27	22.76
930117															
CH.01	N42RF	011200	1200	153.5	90.2	26.47	23.55	-	-	-	-	156.1	90.1	26.51	23.57
EI.01	N308D	011000	900	58.7	89.7	27.54	23.58	64.9	89.7	27.50	23.55	-	-	-	-
930118															
CH.01	N42RF	005900	1000	61.9	270.0	27.66	23.32	-	-	-	-	63.0	270.0	27.79	23.34
CH.02	N42RF	012700	1200	140.9	89.6	26.44	23.42	-	-	-	-	143.0	89.6	26.59	23.41
EI.01	N43RF	010000	900	155.5	270.2	26.51	23.52	159.1	270.2	26.51	23.48	-	-	-	-
930128															
EF.01	N308D	234625	30	60.4	0.9	27.98	18.50	60.7	355.1	28.38	23.89	-	-	-	-
EF.02	N308D	000300	30	61.6	179.5	28.04	18.50	64.7	180.6	28.45	23.82	-	-	-	-
930201															
HI.01[b]	N43RF	212500	1200	n.a.	270.1	28.12	23.14	-	-	-	-	62.5	269.8	28.08	23.21
HI.02[b]	N43RF	215300	1000	n.a.	89.0	27.30	22.62	-	-	-	-	150.5	89.4	27.30	22.67

[a]The flight ID corresponds to the UTC date (YYMMDD) of take-off. Aircraft abbreviations: C130 C, 340A F, N308D E, N42RF H, and N43RF I.

[b]N43RF 1-IIz data tape recorder failed.

and A1c. Adjusting the N42RF radar altitude data by -4 m (section 2.1.1) removes the leadaircraft dependence in the N42RF-N43RF comparison runs (Figure A1c; compare the dashed and solid lines). When N43RF is the lead aircraft (thick lines) there appeared to be many times when N42RF was flying in the lead. This seemingly impossible situation is possible because the trailing aircraft was identified as the one that varied the track angle most. The reason why N42RF would appear to be flying in front of the lead aircraft is that time differences between the onboard computers appear as spatial differences when the relative po-

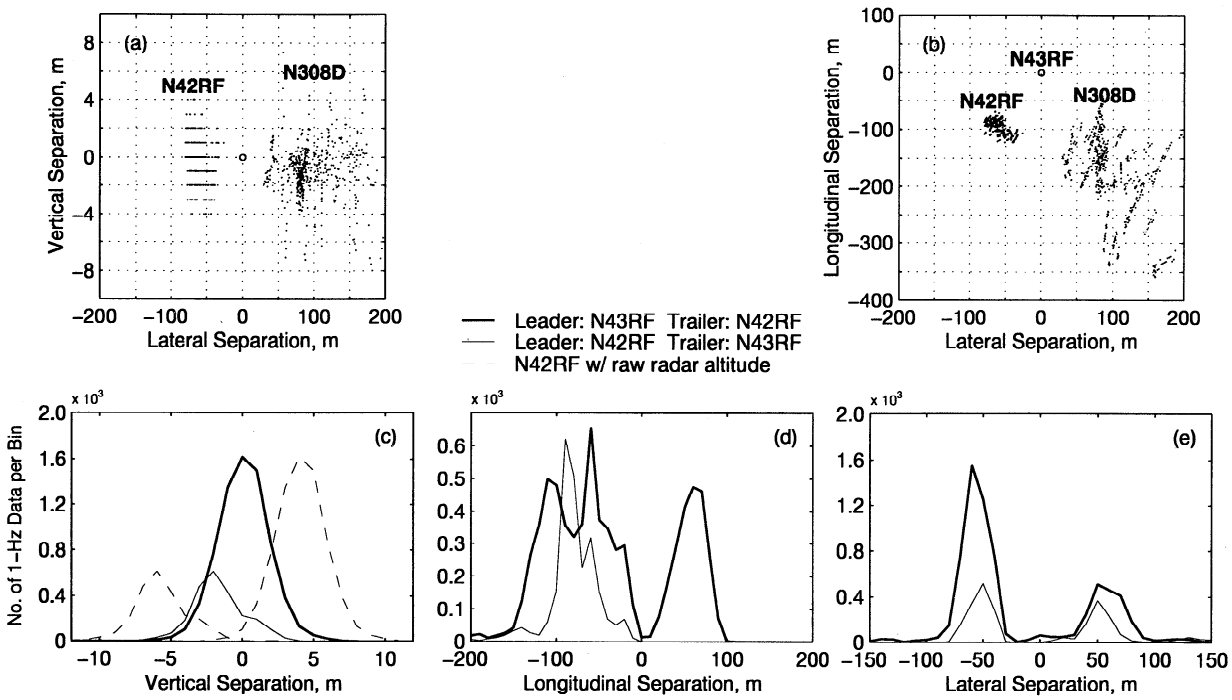

Figure A1. Aircraft positions relative to the lead aircraft (N43RF) during a three-aircraft comparison leg (921126.EHI.01) showing (a) vertical and (b) longitudinal separations versus lateral separation in the N43RF coordinate system. Frequency distributions of all comparison legs between N42RF and N43RF for (c) vertical (positive values indicate trailing aircraft higher), (d) longitudinal (negative values mean the trailing aircraft behind lead aircraft), and (e) lateral (positive means trailing aircraft is on starboard side of the leader) separations. The leading aircraft is identified by line thickness.

sitions are compared. Closer inspection of these data revealed that all the data collected when N42RF was actually trailing (but appeared to be flying in front of the lead aircraft) occurred on 921113. It may be that for some unknown reason the computer clocks differed on that day by 1-2 s. In-flight time checks of clocks between the aircraft revealed that such differences did occur. From other aircraft-aircraft comparisons involving N308D (not shown here), time differences were observed to occur. The relative positions in the lateral direction would not be so seriously affected by any time differences in the clocks. Figure A1e shows that N42RF and N43RF both flew to the starboard and portside of the leading aircraft.

Appendix B: Surface Platform Data Details

B1. Data Sources

Much of the surface-platform data can be obtained from the Center for Ocean Atmospheric Prediction Studies (COAPS) surface meteorology data center at Florida State University. At COAPS the surface platform data have been checked for errors and put into a standard format. Either netCDF or ASCII data are available. There is also a data-quality report for each data set available there. The data used in our study were from a variety of sources, as shown in Table B1. Some of these data were obtained directly from the data processor but may also be available elsewhere.

B2. Aircraft-Surface Platform Comparison Details

Many of the aircraft-surface platform comparisons were purposely flown on dedicated intercomparison missions and logged on flight notes by investigators. However, due to the large number of platforms and vast amount of data involved, a postflight technique based on navigation data from the various platforms has been developed to systematically identify all possible aircraft-surface platform intercomparisons.

Conceptually, a surface-platform overflight could be described as a straight and level aircraft run that crosses an imaginary vertical cylinder centered on the surface-platform location and whose radius R and height H are the maximum allowable aircraft-to-surface-platform horizontal separation and aircraft height, respectively. On the basis of an Earth radius value appropriate for the equatorial region, the aircraft-to-surface-platform distance r was estimated using GPS-corrected latitude and longitude measurements from the inertial navigation unit on the aircraft. Over the ocean (no topography) and at low levels, aircraft altitude h is more accurately measured by radar altimeters, therefore elevation

Table B1. Acquisition Details of TOGA COARE Surface Platform Data

Platform	Data Type/SI	Data Processor	Release Date
R/V *Franklin*	ASCII (15 min)	FSU/COAPS, CSIRO	November 29, 1995[a]
R/V *Wecoma*	ASCII (30 min)	FSU/COAPS, OSU/COAS	August 1, 1995[b]
	ASCII (1 min)	OSU/COAS	April 1, 1994[c]
R/V *Moana Wave*	ASCII (10 min)	NOAA/ERL	January 1, 1996[d] (release 2.5)
WHOI mooring	ASCII (7.5 min)	WHOI	April 21, 1994[e] (togavawrv4.asc)
ATLAS mooring (mt165a)	ASCII (60 min)	NOAA/PMEL	April 21, 1994[f]

[a]http://www.coaps.fsu.edu:80/coare/; Frank Bradley (frank.bradley@cbr.clw.csiro.au)).
[b]http://www.coaps.fsu.edu:80/coare/; Clayton Paulson (paulson@oce.orst.edu).
[c]Obtained at TOGA COARE International Data Workshop; Clayton Paulson (paulson@oce.orst.edu).
[d]Obtained via anonymous ftp; Chris Fairall (cfairall@etl.noaa.gov).
[e]Obtained via anonymous ftp; Robert Weller (rweller@whoi.edu).
[f]Obtained via anonymous ftp; Meghan Cronin (cronin@pmel.noaa.gov).

data from these instruments were used. The value of H and R was set to 100 m and 6 km, respectively. In some instances (mostly for comparisons involving ATLAS and *Wecoma*), R was increased to 15 km to include more comparison points.

Following these criteria, the screening of all available data resulted in 267 overflights. Of these, 73% had $r < 5$ km and 87% had $r < 8$ km as revealed by the histogram of Figure B1b. It can also be seen on the histogram of h of Figure B1a that most of the intercomparisons are clustered at three flight levels: 33, 63, and 92 m. A detailed inventory, wherein all selected intercomparisons between the aircraft and the surface platforms were sorted by UTC date, is given in Figure B2. It shows that many of these comparisons occurred on the dedicated intercomparison dates (November 27-28 and January 9-10).

For a given overflight, the coincidence time was the UTC time (to the nearest second) at which the aircraft was closest to the surface platform considered. Because the aircraft data used in this study were sampled at a much higher rate than were the surface-platform data (see Table 1), the latter were interpolated using a cubic spline method. The averaging period of the aircraft

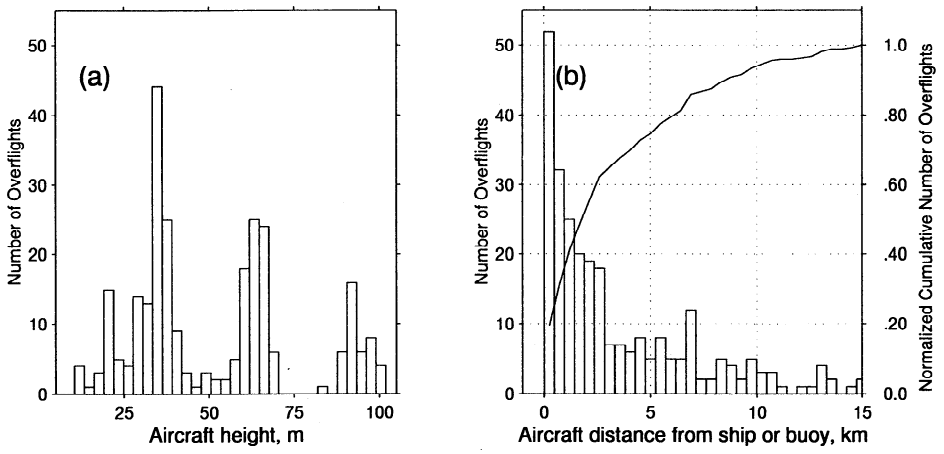

Figure B1. Histogram of (a) aircraft mean elevation and (b) horizontal separation between aircraft and surface platforms from the 267 aircraft overflight time periods. The normalized cumulative number of comparisons is shown on the right axis of (b).

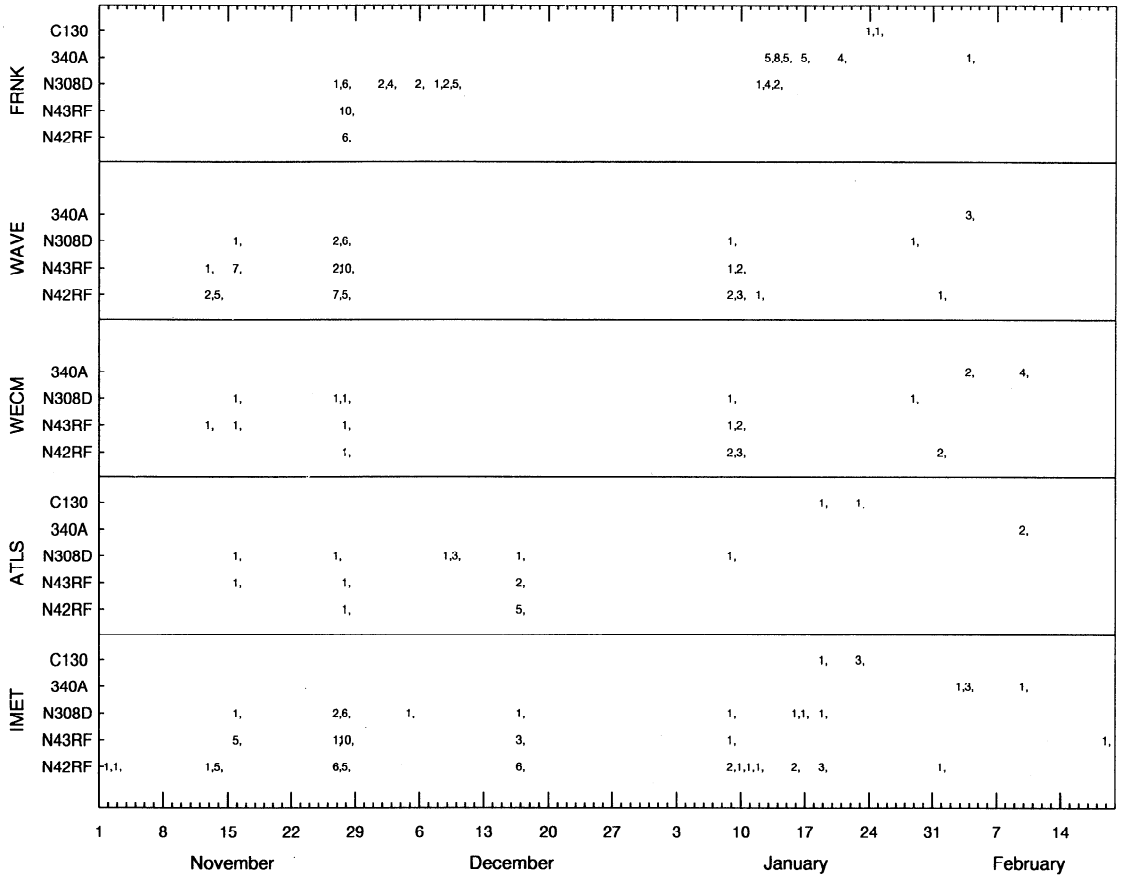

Figure B2. Number of comparison occurrences between each aircraft and each surface platform versus UTC date (for clarity a comma has been added after each number).

data was determined using Taylor's hypothesis of frozen turbulence. On the basis of the mean wind speed V for a given run, the distance traveled by an air parcel past a surface platform during the surface-platform-data averaging time Δt is $d = V\Delta t$. The time it takes an aircraft to cover that distance is d/U (U is the mean true airspeed of the aircraft on that run), which was used for the aircraft data averaging period. Aircraft data means calculated over 100 s ($\sim$ 10 km) segments were found to be very close to those obtained from the V- and U-dependent averaging periods.

Acknowledgments. We acknowledge all participants in the massive, multinational, TOGA COARE data collection period. We especially appreciate the long hours spent collecting data by flight crews and ship personnel aboard the NOAA WP-3Ds, NCAR N308D, FIAMS 340A, MRF C130, R/V *Franklin*, R/V *Moana Wave*, and R/V *Wecoma*, as well as those involved in the IMET and ATLAS buoy deployments. Helpful discussions about these data occurred within the TOGA COARE Air-Sea Flux Science Group; we particularly thank Peggy LeMone, Xilong Song, Bryan Hannegan, Denise Hagan, Yolande Serra, Mike McPhaden, Dean Vickers, and Lynn deWitt for their contributions. We also appreciate the data archiving and quality-control checks performed by David Legler and staff at the Surface Meteorology Data Center, Florida State University. We also thank two anonymous reviewers for their helpful comments. The work of S.P.B., D.K., and C.A.F. was supported by NSF grants ATM-9024436 and ATM-9110540, and NOAA grant 56GP0154-01. R.A.W. and S.P.A. were supported by NSF grant ATM-9525844. C.A.P. was supported by NSF grant OCE-9113510. This is WHOI contribution 9836.

References

Anderson, S. P., and M. F. Baumgartner, Radiative heating errors in naturally ventilated air temperature measurements made from buoys, *J. Atmos. Oceanic Technol.*, *15*, 157-173, 1998.

Beardsley, R. C., A. G. Enriquez, C. A. Friehe, and C. A. Alessi, Intercomparison of aircraft and buoy measurements of wind and wind stress during SMILE, *J. Atmos. Oceanic Technol.*, *14*, 969-977, 1996.

Brown, E. N., Position error calibration of a pressure survey aircraft using a trailing cone, *NCAR Tech. Rep. TN-313+STR*, 29 pp., Natl. Cent. for Atmos. Res., Boulder, Colo., 1988.

Businger, J. A., J. C. Wyngaard, Y. Izumi, and E. F. Bradley, Flux profile relationships in the atmospheric surface layer, *J. Atmos. Sci.*, *28*, 181-189, 1971.

Cronin, M. F., and M. J. McPhaden, The upper ocean heat balance in the western equatorial Pacific warm pool during September-December 1992, *J. Geophys. Res.*, *102*, 8533-8553, 1997.

Dobosy, R. J., T. L. Crawford, J. I. MacPherson, R. L. Desjardins, R. D. Kelly, S. P. Oncley, and D. H. Lenschow,

Intercomparison among four flux aircraft at BOREAS in 1994, *J. Geophys. Res., 102*, 29,101-29,111, 1997.

Fairall, C. W., E. F. Bradley, J. S. Godfrey, G. A. Wick, J. B. Edson, and G. S. Young, The cool skin and warm layer in bulk flux calculations, *J. Geophys. Res., 101*, 1295-1308, 1996a.

Fairall, C. W., E. F. Bradley, D. P. Rogers, J. B. Edson, and G. S. Young, Bulk parameterization of air-sea fluxes for Tropical Ocean-Global Atmosphere Coupled Ocean-Atmosphere Response Experiment, *J. Geophys. Res., 101*, 3747-3764, 1996b.

Friehe, C. A., R. C. Beardsley, C. D. Winant, and J. P. Dean, Intercomparison of aircraft and surface buoy meteorological data during CODE-1, *J. Atmos. Oceanic Technol., 1*, 79-86, 1984.

Godfrey J. S., R. A. Houze, R. H. Johnson, R. Lukas, J.-L. Redelsperger, A. Sumi, and R. A. Weller, Coupled Ocean-Atmosphere Response Experiment (COARE): An interim report, *J. Geophys. Res., 103*, 14,395-14,450, 1998.

Grant, A. L. M., and P. Hignett, Aircraft observations of the surface energy balance in TOGA-COARE, *Q. J. R. Meteorol. Soc., 124*, 101-122, 1998.

Hoaglin, D. C., F. Mosteller, and J. W. Tukey, *Understanding Robust and Exploratory Data Analysis*, 447 pp., John Wiley, New York, 1983.

Khelif, D., S. P. Burns, and C. A. Friehe, Improved wind measurements on research aircraft, *J. Atmos. Oceanic Technol., 16*, 860-875, 1999.

Lambert, D., and P. Durand, Aircraft to aircraft intercomparison during SEMAPHORE, *J. Geophys. Res., 103*, 25,109-25,123, 1998.

LeMone, M. A., and W. T. Pennell, A comparison of turbulence measurements from aircraft, *J. Appl. Meteorol., 19*, 1420-1437, 1980.

LeMone, M. A., E. J. Zipser, and S. B. Trier, The role of environmental shear and thermodynamic conditions in determining the structure and evolution of mesoscale convective systems during TOGA COARE, profile relationships in the atmospheric surface layer, *J. Atmos. Sci., 55*, 3493-3518, 1998.

Lenschow, D. H., and P. Spyers-Duran, Measurement techniques: Air motion sensing, *NCAR Res. Aviat. Facil. Bull. 23*, 36 pp., Natl. Cent. for Atmos. Res., Boulder, Colo., 1989.

Liepmann, H. W., and A. Roshko, *Elements of gasdynamics*, 439 pp., John Wiley, New York, 1957.

MacPherson, J. I., R. L. Grossman, and R. D. Kelly, Intercomparison results for FIFE flux aircraft, *J. Geophys. Res., 97*, 18,499-18,514, 1992.

Miller, E. R., and R. B. Friesen, Standard output data products from the NCAR research aviation facility, *NCAR Res. Aviat. Facil. Bull. 9*, 9 pp., Natl. Cent. for Atmos. Res., Boulder, Colo., 1989.

Nicholls, S., An observational study of the mid-latitude, marine, atmospheric boundary layer, 307 pp., Ph.D. thesis, Univ. of Southampton, England, 1983.

Nicholls, S., W. Shaw, and T. Hauf, An intercomparison of aircraft turbulence measurements made during JASIN, *J. Clim. Appl. Meteorol., 22*, 1637-1648, 1983.

Rockwood, A. A., A. H. Miller, C. E. Duchon, and A. J. Koscielny, Analysis and results from the GATE tower flybys and aircraft intercomparisons of the thermodynamic variables from the U.S. Electra, DC-6, and the U.K. C-130, *NCAR Tech. Rep.*, 71 pp., Natl. Cent. for Atmos. Res., Boulder, Colo., 1977.

Serra, Y. L., D. P. Rogers, D. E. Hagan, C. A. Friehe, R. L. Grossman, R. A. Weller, and S. P. Anderson, Atmospheric boundary layer over the central and western equatorial Pacific Ocean observed during COARE and CEPEX, *J. Geophys. Res., 102*, 23,217-23,237, 1997.

Stuart, D. W., R. J. Goodwin, and N. P. Duval, A comparison of surface winds and wind measurements at 152 m during JOINT I, 1974, and JOINT II, 1977, *Coastal Upwelling*, edited by F.A. Richards, pp. 39-43, AGU, Washington, D. C., 1981.

Webster, P. J., and R. Lukas, TOGA COARE: the coupled ocean-atmosphere response experiment, *Bull. Am. Meteorol. Soc., 73*, 1377-1416, 1992.

Weller, R. A., and S. P. Anderson, Surface meteorology and air-sea fluxes in the western equatorial Pacific warm pool during the TOGA Coupled Ocean-Atmosphere Response Experiment, *J. Clim., 9*, 1959-1990, 1996.

Williams, A. G., and J. M. Hacker, Description of instrumentation and flights conducted with FIAMS Cessna 340A aircraft "EOS" during the international experiment TOGA COARE, *Flinders Inst. Atmos. Mar. Sci. Tech. Rep. 10*, 65 pp., Flinders Univ. of South Australia, Adelaide, Australia, 1993.

S. P. Anderson and R. A. Weller, Physical Oceanography Department, MS 29, Woods Hole Oceanographic Institution, Woods Hole, MA 02543-1541. (sanderson@whoi.edu, rweller@whoi.edu,)

E. F. Bradley, CSIRO Land and Water, GPO Box 1666, Canberra, ACT 2601, Australia. (frank.bradley@cbr.clw.csiro.au)

S. P. Burns, C. A. Friehe, and D. Khelif, Department of Mechanical and Aerospace Engineering, University of California, Irvine, CA 92697-3975. (sean@wave.eng.uci.edu; cfriehe@uci.edu; dkhelif@uci.edu)

M. F. Cronin, Pacific Marine Environmental Laboratory, NOAA, 7600 Sand Point Way NE, Seattle, WA 98115-0070. (cronin@pmel.noaa.gov)

C. W. Fairall, Environmental Technology Laboratory, NOAA, 325 Broadway, Boulder, CO 80303-3328. (cfairall@etl.noaa.gov)

A. L. M. Grant and A. G. Williams, Hadley Centre for Climate Prediction and Research, U.K. Meteorological Office, London Road, Bracknell, Berkshire RG12 2SY, United Kingdom. (almgrant@meto.gov.uk, awilliams@meto.gov.uk)

J. M. Hacker, Flinders Institute for Atmospheric and Marine Sciences, Flinders University, GPO Box 2100, Adelaide, SA 5001, Australia. (j.hacker@es.flinders.edu.au)

P. Hignett, Meteorological Support Group/DG(R&T), Ministry of Defence, Whitehall, London SW1A 2HB, United Kingdom. (phignett.msg.mod@gtnet.gov.uk)

C. A. Paulson, College of Oceanography, Oregon State University, Corvallis, OR 97331-5503. (paulson@oce.orst.edu)

D. P. Rogers, Marine Meteorology Research Group, Scripps Institution of Oceanography, La Jolla, CA 92093-0230. (drogers@ucsd.edu)

(Received October 12, 1998; revised August 23, 1999; accepted August 31, 1999.)